The design, instrumentation, and validation of a multiphase shock tube facility

---

A Thesis presented to

the Faculty of the Graduate School

at the University of Missouri-Columbia

In Partial Fulfilment

of the Requirements for the Degree

Masters of Science

---

by

CONSTANTINE GREGORY AVGOUSTOPOULOS

Dr. Jacob A. McFarland, Thesis Supervisor

May 2017

The undersigned, appointed by the Dean of Graduate School, have examined the thesis entitled:

THE DESIGN, INSTRUMENTATION, AND VALIDATION OF A MULTIPHASE SHOCK TUBE FACILITY

presented by Constantine Gregory Avgoustopoulos,

a candidate for the degree of Master of Science and hereby certify that, in their opinion,

it is worthy of acceptance

_____

Dr. Jacob A. McFarland

_____

Dr. Josiah A. Bryan

_____

Dr. Scott Kovaleski

Acknowledgments

My career as a Masters student has been one of the biggest challenges of my life. There are countless people who have helped me in getting this far in my life goals. I would first like to thank my advisor, Dr. Jacob McFarland. His selfless character has gone above and beyond in guiding me through my many difficulties I faced doing research as a graduate student. He has given me a great opportunity in this research field, that I otherwise never would have thought I would experience. It has been an absolute privilege to work for him. Additionally, I would like to thank my committee member Dr. Josiah Bryan and Dr. Scott Kovaleski, who have taken the time to review my work and provide feedback.

I would like to thank my lab mates Wolfgang Black and Jeevan Dahal. They helped me both in the lab and in the classroom and provided me guidance in becoming a better researcher. Raj Kothakapa, his patience and willingness to compromise is a true show of character. Roy Allen whose practicality and hard work ethic is something I admire. Manoj Paudel provided me with the moral support through my thesis. The undergrads John Middlebrooks and Daniel Ratigan providing the assistance that was needed to accomplish the goals of the lab.

I would also like to thank my friend and former lab mate Justin White who not only assisted me in the lab but also helped me in my transition Columbia from knowing nobody, to introducing me to his friends and making me feel at home. Jake Strope and Sam Kreter's great sense of humor and personality made living in Columbia that much better.

Finally I must thank my family. My mother and father have provided me with the moral support I needed to make it through my undergraduate and graduate studies. They taught me the importance of self reliance and have shaped me into the man I am today, I owe them a great deal for my success. My sister has been a source of humor when the times were tough. My brother who always welcomed me with open arms when I would visit home.

Contents

Acknowledgments ii

List of Figures v

Abstract vii

1 Introduction 1

1.1 Motivation 1

1.2 Theory 2

1.3 Literature Review 6

2 Shock Tube Facility Design 10

2.1 Pressure Gradient 10

2.1.1 Driver 13

2.1.2 Driven 15

2.1.3 Test Section 18

2.1.4 Bolted Connection 21

2.1.5 Diaphragm Loader Design 23

2.2 Density Gradient 26

2.2.1 Interface Pieces 26

2.2.2 Particle Delivery system 27

2.3 Instrumentation, Control, and Visualization 28

2.3.1 Dynamic Pressure Transducers 28

2.3.2 Control Valve System 30

2.3.3 Control and Measurement system 32

2.3.4 Window Design 33

2.3.5 Laser and Camera 36

2.4 Facility capabilities 39

3 Preliminary experiments in the shock tube **40**

3.1 Initialization and calibration 41

3.2 Experimental Methods 45

3.3 Qualitative observations of interface evolution 46

3.3.1 Low Particle Atwood Number 46

3.3.2 High Particle Atwood Number 49

3.4 Quantitative observations of interface evolution 52

4 Conclusion and Summary **54**

Bibliography **56**

List of Figures

1.2.1 comparison of a classical RMI (a,b,c) to a SDMI (d,e,f). 4
2.1.1 Completed Shocktube 11
2.1.2 Diagram of the shock tube pre-shock (a), Post-shock (b), and detail of reshock in the test section (c). 12
2.1.3 Solidworks FEA analysis of driver at 2200 psi 14
2.1.4 Socket-weld flange with driver 15
2.1.5 FEA simulation of Driver blank at 2200 psi 16
2.1.6 FEA simulation of Socket-weld flange at 2200 psi 16
2.1.7 FEA simulation of Driven at 600 psi 17
2.1.8 FEA simulation of square flange at 600 psi 18
2.1.9 a) 8 bolt pattern and b) 12 bolt pattern 19
2.1.10 Test section 20
2.1.11 Detail of interface creation section 20
2.1.12 FEA simulation of test section at 600 psi 21
2.1.13 FEA simulation of blank flange at 600 psi 22
2.1.14 Diaphragm before experiment (left) after experiment (right) 23
2.1.15 SolidWorks model of diaphragm flange 24
2.1.16 SolidWorks model of CSC flange 25
2.1.17 Diaphragm loader disassembled (left) assembled (right) 25
2.2.1 Gas Cylinder as viewed from the Vertical Plane (top) and the Center Plane (bottom). 26
2.2.2 gas cylinder interface nozzle 27
2.2.3 Particle distribution created in nebulizers (left) and interferogram of a single particle (right) 29
2.3.1 Custom made fitting for DPT and commercially available NPT plug 30
2.3.2 Gas delivery system 31

2.3.3 Machined surface of TS with window hole 34
2.3.4 SolidWorks model of window assembly 35
2.3.5 FEA of window cover at 600 psi (left) and acrylic window (right) 36
2.3.6 Diagram of laser setup 38
2.3.7 Camera oriented horizontally on Shock Tube 39
2.3.8 Camera oriented vertically on Shock Tube 39
3.1.1 Diagram of interface creation system 42
3.1.2 Initial condition of interface using PIV 44
3.3.1 Mosaic of evolving interface with low atwood number 47
3.3.2 Comparison of simulation and experimental result for a low Atwood number 48
3.3.3 Mosaic of evolving interface 49
3.3.4 Detail of interface at 2.1ms 51
3.3.5 Detail of colliding particle filaments developing at 4.0ms 51
3.4.1 PIV processed image of shocked interface at 2.9ms 53

Abstract

This paper investigates the experimental work in Shock Driven Multiphase Instabilities (SDMI). SDMIs occur when an interface consisting of a particle seeded gas is instantaneously accelerated and begins mixing. SDMIs have similar flow morphologies to the Richtmyer-Meshkov Instability (RMI), however, the driving force inducing this flow is very different. SDMIs occur when there is a relative velocity difference between surrounding gas and the moving particles. This results to a shear at the edges and ultimately leads to rollups that are similar to a RMI. To investigate this phenomena, a shock tube facility was designed, calibrated, and tested to perform experiments.

The experimental data was qualitatively compared to simulations performed, as well as to literature of similar experiments. Quantitative data was analyzed using Particle Imaging Velocimetry (PIV) to understand the flow of the instability. The flow morphologies observed in experiments have similar behavior to those performed in simulations. Additionally, the qualitative observations of experiments performed in this lab are also in agreement with experimental literature.

Two different effective Atwood numbers are investigated in this study. The first case looks at a gas cylinder interface with an effective Atwood number of -0.01 and a gas Atwood number of -0.02, shocked with a Mach 1.66 shock wave. The observations show a dominating instability resulting in the gas Atwood number. What ends up happening is the smaller particles are pulled into the vortex and the large particles separate and trail behind.

The second case looks at the same gas cylinder perturbation but with an effective Atwood number of 0.03 and a gas Atwood number of 0, shocked at Mach 1.66. The higher Atwood number was achieved by modifying the experimental apparatus slightly to deliver a greater number of particles to the shock tube. The experiments observed show that there is agreement with literature and simulations. Certain unusual filaments begin forming at late times, 4.0ms after shock. This was thought to only appear in a pure RMI. In the case of a SDMI, these filaments are a result of colliding particles.

1 Introduction

1.1 Motivation

The purpose of this work is to present the research, design, and experiments that were performed to study shock driven multiphase instabilities (SDMI). Chapter 1 will cover the background information about SDMIs drawing comparisons to the Richtmyer-Meshkov Instability (RMI), the theory of 1-D Gas dynamics, and a literature review. Chapter 2 will talk about the design of the entire shock tube facility. Chapter 3, will discuss the experimental work performed in the facility. Chapter 4 will summarize the thesis and discuss future work for the shock tube facility.

SDMIs are a challenging field of hydrodynamics. The addition of multiphase components, phase change, and shock waves into the system complicates the flow studied. SDMIs can however be understood by drawing comparisons to the RMI[1, 2], which is a multi-species, single phase shock driven instability and will be discussed later in this paper. SDMIs have applications in various fields of science. In astrophysics for example, the interstellar medium is made up of various types of dust and gas. Shock waves caused by supernovae can interact with these gases and particles. This can potentially begin the very formation of stars and planetary systems by inducing mixing of dust and gas [3, 4]. Another application is the supersonic mixing of fuel in scramjets during startup. As the vessel travels through the air at supersonic speeds, shock waves enter the intake, this shockwave, interacting with the liquid fuel and air increases the rate at which the mixing occurs [5]. In pulse detonation engines (PDE), a pulse generator located inside the engine internally shocks liquid fuel which induces a rapid mixing [6, 7, 8] SDMIs appear in various natural occurrences such as gas turbines [9] as well as the study of the properties of shock induced ejecta particles in the case of high energy explosions. Volcanic eruptions, for example, form complex interactions of particles with liquid and gases which results in the formation of Tephra, or fragmented rock material created by volcanoes [10, 11].

1.2 Theory

Shock driven multiphase instabilities are similar to a well-known phenomena, the Richtmyer-Meskhov instability. To better understand SDMIs, an understanding of the RMI is required. The RMI is a hydrodynamic instability that occurs when two fluids of different densities are instantaneously accelerated and begin mixing. This was first analyzed computationally by Robert Richtmyer, in which he theorized that an instability can be achieved by accelerating a Rayleigh-Taylor unstable interface with a shock wave [1]. Meshkov provided the first experimental proof of Richtmyer's predictions [2]. In fact, before it's namesake the RMI was originally called a "Shocked Accelerated Rayleigh-Taylor Instability (RTI)". The difference between an RMI and RTI is the acceleration component is instantaneous for an RMI, whereas the RTI is sustained constant acceleration.

The RMI can be understood through the vorticity equation (1.2.1)

$$\frac{D\omega}{Dt} = \vec{\omega} \cdot \vec{\nabla} \vec{u} + \nu \nabla^2 \vec{\omega} + \left[\frac{1}{\rho^2} \vec{\nabla} \rho \times \vec{\nabla} P \right]_{Baroclinic\ term} \tag{1.2.1}$$

Where ω is the vorticity, ν is the kinematic viscosity, P is the pressure, ρ is the density, and u is the velocity. To achieve a RMI, three things need to happen. There needs to be a pressure gradient, a density gradient, and a misalignment of the two component vectors. This can be seen in the bracketed section of equation 1.2.1, which is referred to as the baroclinic term. The baroclinic term is the only important term when the density gradient is accelerated instantaneously. The vorticity deposition is directly related to the magnitude of the pressure and density gradients. The pressure gradient is represented by the Mach number, which is defined as the ratio of the flow velocity and the local speed of sound. A higher Mach number results in a greater pressure gradient, leading to greater vorticity deposition in the interface. The second component, the density gradient is represented by the Atwood number (1.2.2). The Atwood number is the ratio of densities between two gases.

$$A = \frac{\rho_1 - \rho_2}{\rho_1 + \rho_2} \tag{1.2.2}$$

Here ρ_1 is the density of the heavier gas and ρ_2 is the density of the lighter gas. The greater the density gradient between the two fluids the greater the vorticity deposition.

SDMIs are different from the RMI in that a pure RMI is a multispecies, single phase system and a pure SDMI is a single species, multiphase system. In other words, for SDMI there is no density gradient of the gas phase, only an effective multiphase density gradient. This is due to the particles seeded into the gas. For example, there are nitrogen-water particle density gradients or air-glycol particle density gradients. This is distinct to an RMI where the gases used are different densities, such as a sulfur hexafluoride(SF_6)-nitrogen interface or a helium-nitrogen interface. Equation 1.2.1 therefore is not adequate in mathematically representing a SDMI. The enstrophy transport equation, seen in equation 1.2.3, represents all of the dissipation effects related to rotational kinetic energy in the flow model. Where ϵ is the void fraction and has to be accounted for when particles are present in a fluid and F_k is the particle momentum source term.

$$\begin{aligned} d_t \frac{\omega_i \omega_i}{2} + u_{g,j} \partial_j \frac{\omega_i \omega_i}{2} = & \left[\omega_i \frac{1}{\rho_g^2} \epsilon_{ijk} \partial_j \rho_g \partial_k P \right]_B + \omega_i \omega_j \partial_j u_{g,i} - \omega_i \omega_i \partial_j u_{g,j} \\ & + \nu \partial_j \partial_j \frac{\omega_i \omega_i}{2} - \nu \partial_j \omega_i \partial_j \omega_i + \left[\frac{1}{\rho_g \bar{\epsilon}} \omega_i \epsilon_{ijk} \partial_j F_k \right]_M \end{aligned} \tag{1.2.3}$$

The important terms here are the baroclinic term B, and the particle multiphase source term M. In a SDMI the baroclinic term is negligible since there is no gas density gradient at the interface, the production of enstropy is driven only by the multiphase source term. The Atwood number can also be modified slightly for application to multiphase systems. This Atwood number will be referred to as the effective Atwood number and can be defined using equation 1.2.4, Where A_{eff} is the effective Atwood number, ρ_{e1} represents the effective density of the test gas, and ρ_{e2} is the effective density of the surrounding gas.

$$A_{eff} = \frac{\rho_{e1} - \rho_{e2}}{\rho_{e1} + \rho_{e2}} \tag{1.2.4}$$

The differences between a SDMI and the RMI can be visually understood from figure 1.2.1. The flow morphology of a RMI and a SDMI look similar, however the driving mechanism that is responsible for these observations is different. In a RMI the physical mechanism is the misalignment of the density and pressure gradient, i.e. when you take the cross product of $\nabla\rho$ and ∇P [1, 2]. For a multiphase system the particle source term is responsible for the instability observed [12]. When the particles are initially shocked, they lag behind the carrier gas in which they are seeded. As the particles reach equilibrium their average velocity, δu_p, is less than that of the surrounding gas, δu_g, this leads to a shear acting on the edges of the particle interface and begins to rollup.

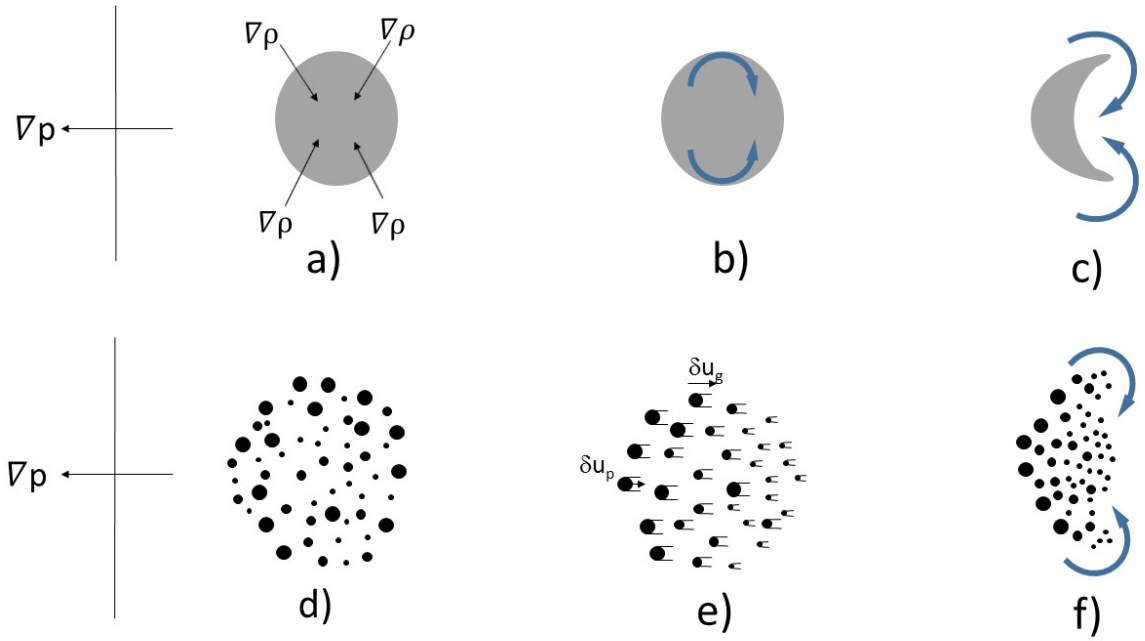

Figure 1.2.1: comparison of a classical RMI (a,b,c) to a SDMI (d,e,f).

Understanding the particles ability to reach equilibrium with the carrier gas requires another definition, the momentum relaxation time t_v and is given by 1.2.5. When the relaxation time is low the particles will respond faster to changes in the fluid flow, i.e the

lag time is shorter

$$t_v = \frac{m_p}{6\pi r_p \mu_{gp}} \tag{1.2.5}$$

The discussion thus far has been about the density gradient. The next important component in a SDMI is the pressure gradient, this is in the form of a shock wave. Shock waves can be created in a shock tube. A shock tube experiment can be simplified as a 1-D gas dynamics problem. The following equations can be used to find properties of gases at different conditions, the wave speed, and the Mach number. The subscripts 1, 2, 3, 4, and 5 denote pre-shock, post-shock, post shock expansion fans from the driver, the driver conditions, and reshock respectively. The sound speed in a given medium can be found using equation 1.2.6, where γ is corresponding ratio of specific heats and can be found in tables [13], R is the gas constant, and T is the temperature of the gas at the given state.

$$\alpha = \sqrt{\gamma R T} \tag{1.2.6}$$

State 4 (the high pressure region) and state 1 (the low pressure region) are separated by a diaphragm. The ratio $\frac{p_4}{p_1}$ is called the diaphragm pressure ratio, this ratio along with γ_1 and γ_4 determines the strength of the shock wave once the diaphragm bursts [13]. Knowing the diaphragm pressure ratio, the the shock strength $\frac{p_2}{p_1}$ can be found using equation 1.2.7. All other incident shock properties can be found using 1.2.8 and 1.2.9. The wave speed and Mach number are found using equation 1.2.11 and 1.2.12 respectively, where W is the shock wave speed. Equation 1.2.10 is used to find reshock pressures and is important in the design of a shock tube if it will be used in experiments involving reshock

$$\frac{p_4}{p_1} = \frac{p_2}{p_1}\left\{1 - \frac{(\gamma_4 - 1)(\alpha_1/\alpha_4)(p_2/p_1 - 1)}{\sqrt{2\gamma_1[2\gamma_1 + (\gamma_1 + 1)(p_2/p_1 - 1)]}}\right\}^{-2\gamma_4/(\gamma_4 - 1)} \tag{1.2.7}$$

$$\frac{T_2}{T_1} = \frac{p_2}{p_1}\left(\frac{\frac{\gamma+1}{\gamma-1}+\frac{p_2}{p_1}}{1+\frac{\gamma+1}{\gamma-1}\frac{p_2}{p_1}}\right) \tag{1.2.8}$$

$$\frac{\rho_2}{\rho_1} = \frac{1+\frac{\gamma+1}{\gamma-1}\left(\frac{p_2}{p_1}\right)}{\frac{\gamma+1}{\gamma-1}+\frac{p_2}{p_1}} \tag{1.2.9}$$

$$\frac{p_5}{p_2} = \frac{(3\gamma-1)\frac{p_2}{p_1}-(\gamma-1)}{(\gamma-1)\frac{p_2}{p_1}+(\gamma+1)} \tag{1.2.10}$$

$$W = \alpha_1\sqrt{\frac{\gamma_1+1}{2\gamma}\left(\frac{p_2}{p_1}-1\right)+1} \tag{1.2.11}$$

$$M = \frac{W}{\alpha_1} \tag{1.2.12}$$

It can be seen that the Mach number is directly related to the shock strength ratio. These shock tube equations describe the conditions behind the shock wave. They are useful in designing the experimental facility since they indicate the maximum pressure experienced in the system. Furthermore, the equations allow the operator to estimate where the interface will be at a given time in the experiment.

1.3 Literature Review

Since the study of SDMIs is a relatively new subject, a lot of the research is based off of studying the RMI. Throughout the history of studying the RMI various methods of creating the pressure gradients (shock wave) and density gradients (interface) have been used. One way of creating the pressure gradient is using laser ablation. Laser driven shock waves use multiple lasers focused on a single object made from an ablative material to create a shock wave. The laser is focused on the surface which creates a 3 dimensional spherical shock wave very similar to the ones seen in ICF and super novae explosions. [14, 15]. Robey *et al.* proved to be successful in creating spherical and planar shock waves using this method. A

second method is to use a blast wave in the form of an explosion [16]. Courtney *et al.* used chemical means to create a shock wave, the ignition of the fuel mixture combusts rapidly and expands creating an explosion which drives a shock wave. This is analogous to how a gun works, where the gun powder can be viewed as the fuel mixture that combusts to create a shock wave. The most common and simplest form of creating a shock wave is to use pressure driven means. This uses the instantaneous release of high pressure gas into a region of low pressure gas. The device that utilizes the method of a pressure driven shock wave is called a shock tube. A pressure driven shock tube typically has a diaphragm that separates the high and low pressure regions. There are several methods for breaking the diaphragm. The use of a pneumatically driven plunger with a sharp point has been used to break the diaphragm under pressure [17]. The other method is to use a knife edge that will rupture the diaphragm. This is desirable since it cuts the diaphragm evenly into 4 sections like a flower pedal [18].

The density gradient is achieved by injecting a test gas of different density into an ambient gas of another density. Depending on the type of experiment, the test gas may be more or less dense than the surrounding ambient gas. Jacobs *et al.* for example did experiments with both heavy gas into light gas, using SF_6 and air respectively, and light gas into heavy gas, He and air respectively [19]. One feature of the density gradient is its shape. Different shapes of interfaces yield different results. One example is a varicose gas curtain [20, 21], Orlicz *et al.* used a heavy gas curtain consisting of SF_6 and fog. The experiments used Mach numbers of 1.2 and 1.5. The gas curtain was achieved using a thin wide nozzle with a row of circular holes and small slots cut between each hole. Other perturbations include an inclined interface [22, 23], which is achieved by raising one end of the shock tube while keeping the other end fixed on a pivot so that it creates and angle relative to horizontal. Some labs have performed experiments using a sinusoidal interface perturbation [24]. This can be achieved by using copper plate in the shape of a sine wave that separates the gas density interface. The plate then retracts just before shock arrival creating the sine shape interface. A second

way of creating the same perturbation is to physically move the shock tube using a stepper motor that oscillates at a certain frequency while simultaneously injecting test gas creating a sine wave interface[25].

A simple and extensively studied interface perturbation is a gas cylinder [26, 27, 28, 17, 29, 30, 31, 32]. This was first pioneered by Jacobs studying a single light gas cylinder [26]. His experimental setup used a helium gas cylinder injected into air, all experiments used a Mach 1.093 shock wave. The helium cylinder was mixed with a flourecent tracer to visualize the interface, allowing him to use planar laser induced flourescence (PLIF) measurement techniques. The experiments showed an initial compresseion of the gas cylinder after it was shocked followed by counter rotating vorticies, a result of the misalignment of the pressure gradient from the shock wave and the density gradient at the boundary of the cylinder. In agreement with theory he found that the magnitude of the vorticity is proportional to the product of the pressure and density gradient. He then experimented with heavy gas cylinders [27]. The heavy gas used in these experiments was SF_6 injected into air. The results found similar behavior of mixing gas as it was found in his previous work [26] however since the density gradient was in the opposite direction, inward pointing instead of outward pointing, the counter rotating voticies formed were also in the opposite direction.

In addition to single gas cylinders, there have also been multiple gas cylinders studied [30, 31, 28]. Multiple gas cylinders are quite interesting since they show instabilities not seen in single gas cylinders. One might presume for example, that a side by side 2 gas cylinder interface would result in two identical counter rotating vortex structures. However experimental results show there is a great deal of complexity when more gas cylinders are introduced in an experiment. Factors such as the spacing between the centers of the gas cylinders relative to their diameters are some of the things that affects the evolution of the instability. Tomkins *et al.* [31] used a two gas cylinder arrangement. They varied the center to center distances of the gas cylinders using the relation S/D, where S is the distance from center to center and D is the diameter of the cylinder. They used S/D values from 1.2-2.0,

in other words, they kept the diameter the same but only changed the distances between the cylinders. The two cylinder interface was shocked with a Mach 1.2 shock wave. It was found that for spacings less than 1.4 the evolution of the interface is very different, inward vorticies do not even appear to form. In fact for distances less than 1.4 the two gas cylinders seems to evolve into a single large counter rotating vortex shape, much like the ones seen for a single gas cylinder. This indicates a dominating interaction of the two gas cylinders as the distance between the two is decreased. This thesis, however, only looks into a single gas cylinder for its simplicity.

The discussion up until now has been about creating a density gradient to study the RMI. This paper will now progress in discussing SDMIs. While there is limited experimental research in this subject, it has been performed before. Vorobieff was the first to reproduce experimental results of a SDMI [33]. Using the University of New Mexico shock tube facility, he proved that an instability could be created with shock interaction and a multiphase system alone. Vorobieff used an air particle interface using micron sized glycol and fog particles seeded into air, the effective Atwood number in this case was 0.03. The Mach number in these experiments was 1.66, leading to a 570 m/s wave speed. The flow morphology observed in the multiphase system is similar to that of a heavy gas RMI, namely two counter rotating vortices. However at the microscopic level, the vorticity roll-ups due to the multiphase system appear much weaker than in a heavy gas RMI. Other features that SDMIs lack are the spikes that emerge downstream of the interface, as well as two symmetrical filaments.

Computationally SDMIs were investigated by McFarland *et al.* [12]. This computational study used a particle-gas condition compared with a dusty gas approximation. Here the dusty gas approximation is essentially a classical RMI. The particle-gas case looks at the effects that multiphase particle systems have on the overall flow of the interface. The results showed that for a gas-particle case with particle diameter of 2 μm the circulation rate is 25 percent lower than in a dusty gas approximation. This is due to the particle lag effects. It was concluded that the particle lag is the main reason for this effect. They further

investigated how the particle size affects circulation. Using the dusty gas approximation as a comparison, the particle diameters compared were 0.5, 2, 4.5 and 10 microns. Large particles show considerable lag while also slowing the entire interface down by a small amount. This is due to momentum of the particles; heavier particles are harder to move than lighter particles. Particle size also has an effect on the vortex formation of the shocked interface, larger particles lead to an overall decrease in vortex formation.

None of the aforementioned experiments can be achieved without a proper facility, this information presented in this study will go into great detail about the entire design of the shock tube facility as well as the initial experiments used to validate its capabilities.

2 Shock Tube Facility Design

This is by far the most important and labor intensive portion of the authors work. Without a shock tube facility, experiments could not be undertaken and there would be no study of SDMI. The design, construction, instrumentation, and initial experiments are outlined in this thesis as a reference for future projects.

2.1 Pressure Gradient

The first essential component of a SDMI is the pressure gradient, an impulsive acceleration that is achieved with a shock wave. A commonly used device to deliver the shock wave is called a shock tube. This is used because it allows for experiments to be conducted in a controlled and repeatable manner. The shock tube build for the Mizzou Fluid Mixing and Shock Tube Lab (FMSTL) is shown in figure 2.1.1

Understanding what is actually occurring inside a shock tube experiment is important for the design of a shock tube facility. A simplified diagram of a shock tube can be seen in figure 2.1.2. The shock tube is separated into three main sections. The driver, driven, and test section. The driver section is where gas is delivered to create a pressure differential,

Figure 2.1.1: Completed Shocktube

refereed to as state 4. State 1 represents the low pressure region of the shock tube, (driven and test section). The gas, typically Nitrogen or Helium, is delivered into the driver using a hose. The driver and driven sections are separated by a diaphragm, usually a thin sheet of polycarbonate or metal, this creates a seal within the driver. At a pre-determined pressure in the driver, the diaphragm bursts which creates a propagating shock wave that travels downstream into the driven section. The shock wave creates an instantaneous change in gas conditions whether that be pressure, temperature, density, etc. referred to as state 2. If the shock tube is designed to have the opposite end closed off, the shock wave will reflect off the end and create reshock effects referred to as state 5. When the shock tube end is open the shock wave will simply exit out the end. However, when there is a closed off wall it will reflect and propagate back upstream. When this happens the interface will be shocked a second time and additional mixing occurs, these effects are desirable to observe as they are arise in nuclear fusion and supernovae explosions.

The basic requirements of this facility were investigated. It had to be long enough to

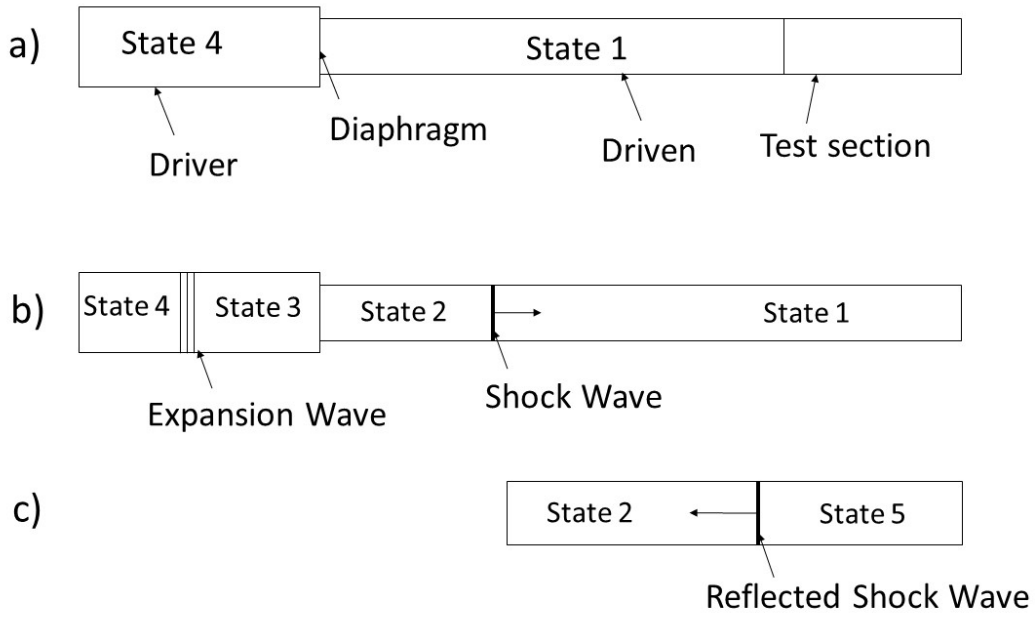

Figure 2.1.2: Diagram of the shock tube pre-shock (a), Post-shock (b), and detail of reshock in the test section (c).

allow for a fully developed shock wave. It had to have the structural capability to withstand a Mach number of 2.5 in atmospheric conditions. Finally, it needed to be versatile to allow for different arrangements of the test section as well as have different interface perturbation options.

The entire shock tube is made from cold formed carbon steel. The reason for using carbon steel over stainless steel is because it is less expensive and stronger. That being said, carbon steel corrodes easily in atmospheric conditions, more so in humid conditions. Proper corrosion protection was needed to ensue that the shock tube could maintain longevity in its service. Several options for corrosion protection were explored including electro plating, painting, and galvanizing. It was decided that due to the ease of operation as well as the relative low cost to produce it, galvanizing was the chosen operation. The outside of the shock tube was also painted all black as well as the insides of the test section to keep light reflections to a minimum while conducting experiments.

2.1.1 Driver

The driver is where the pressure is increased to a desired amount in which a diaphragm bursts. The driver is a 5 foot long, NPS 10 SCH 140 tube, made out of A106 carbon steel. Since the driver will endure the highest pressures in the entire design, it needed to have a circular cross section to reduce stress concentrations. The American Society of Mechanical Engineers (ASME) rates this pipe with a working pressure of 4651 psi and a factor of safety (FoS) of 2 using Barlows formula.

$$P = \frac{2ST}{(D)(FoS)} \tag{2.1.1}$$

Where S is the tensile strength of the material, T is the wall thickness, D is the pipe outside diameter, and FoS is the factor of safety. To verify that the driver could hold up to the pressures in experiments, Finite Element Analysis (FEA) was performed in SolidWorks. For an experiment involving a Mach 2.5 shock wave, the maximum pressure will not surpass 2200 psi in the driver. The results showed that for a pressure of 2200 psi the factor of safety is 3.1. This gives a conservative estimate of the tubes capabilities.

The next task was to design the flanges that would close up the end of the driver. The flanges needed to be made of high strength material to withstand the pressures experienced in the driver. Additionally, the flanges were to be custom made from a local machine shop, this would allow for visits to make sure the fabrication process is running smoothly. Various steels were proposed, A36 steel for example is a commonly used low carbon steel in machining. The problem with this material is the yield strength of 36 ksi, is too low for application in these experiments. It was found that ASTM A514 steel was the best choice for the shock tube flanges since it has a yield strength of 100 ksi and is commercially available. Since the driver will need to contain the highest pressures the flanges here will need to be made with 2 inch thick steel. There were several flange types considered in this design, initially a weld-neck type flange was proposed. These flanges have a tapered neck that are welded on

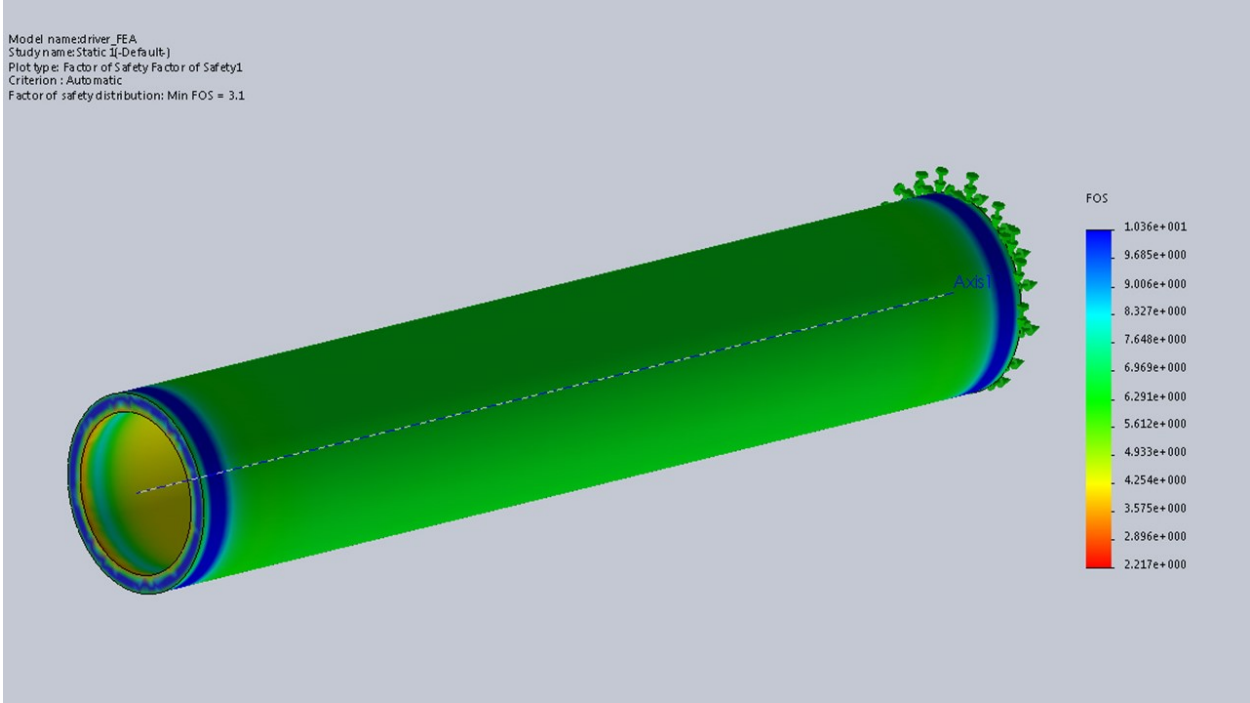

Figure 2.1.3: Solidworks FEA analysis of driver at 2200 psi

to the end of a circular tube. Due to the complexity of the shape, this design would have to be bought and there weren't any flanges available in the material that was required, so the choice was eliminated. A slip-on flange was also proposed due to the simple shape of the flange which is just a disk going over the tube. The problem with this design is the flange has to be welded on the mating face of the shock tube. This would add complexity and matching costs to smooth out the surface of the flange. The socket type flange was the best choice for this design since it only had to be welded on the inside and outside diameter of the tube eliminating the need to machine the mating surface of the flange. The result is a 14 inch diameter, 18 bolt hole circular pattern ensuring a study construction and tight seal. Figure 2.1.4 shows a SolidWorks model of the socket-weld flange used in the driver.

A blank flange is needed to close off the front end of the driver, this piece would contain the pressures that are experienced before a shock is fired. Like the tube in the driver, the blank flange will have to contain 2200 psi, which corresponds to a Mach 2.5 shock wave. FEA simulations were performed on SolidWorks for the flanges. Since the flanges have

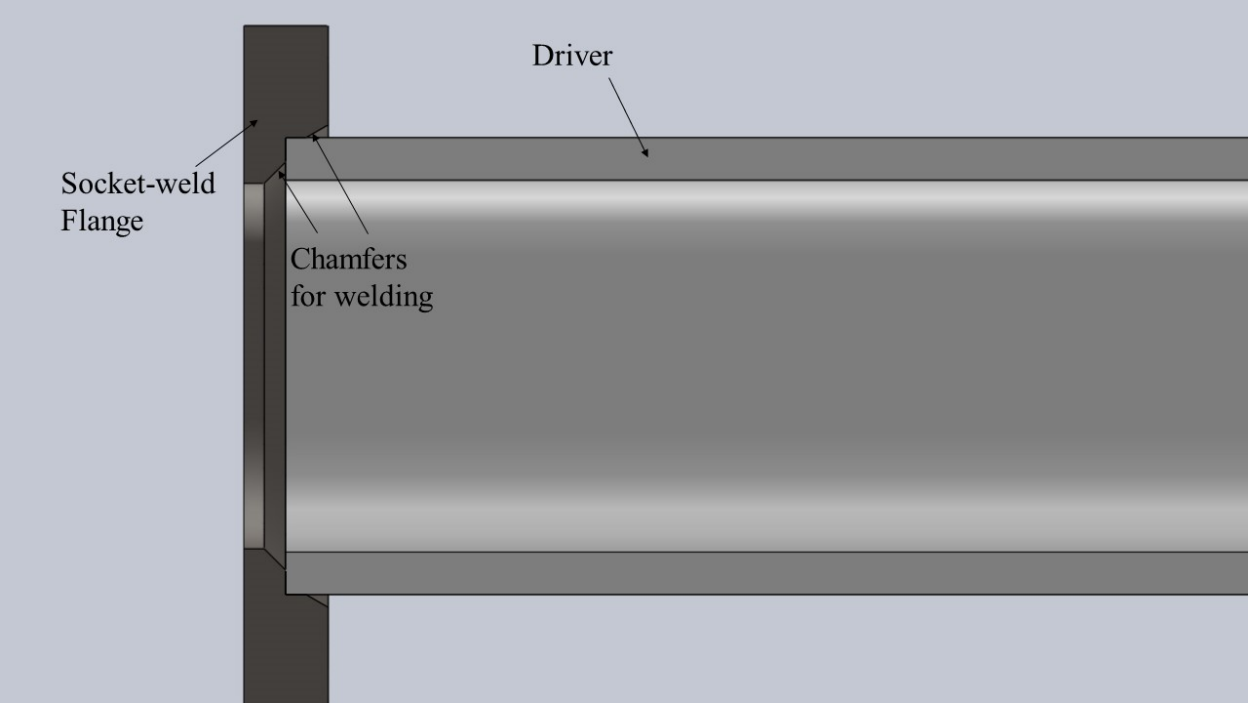

Figure 2.1.4: Socket-weld flange with driver

circular symmetry, the model can be sectioned into a 1/18th segment. When running FEA simulations in SolidWorks the user has the option to select circular symmetry as a constraint. This option assumes the component is symmetric about the axis, but only analyses the 1/18th segment, this saves computational time. The results are shown in figure 2.1.5 and 2.1.6 for the blank flange and socket weld flange, respectively. The FEA results proved that for the thickness and material chosen the factor of safety was 4.4 for the blank flange and 4.4 for the socket-weld flange. The other end of the driver contains the diaphragm flange and will be covered in the next section.

2.1.2 Driven

The purpose of the driven section is to ensure that the compression waves released by the bursting diaphragm develop into a planar shock wave. The driven section is constructed out of two, 8 foot sections that are made from A500 carbon steel. It is a 7 inch x 7 inch square tube with 3/4 inch radius fillets at the corners, with 3/4 inch wall thickness effectively giving

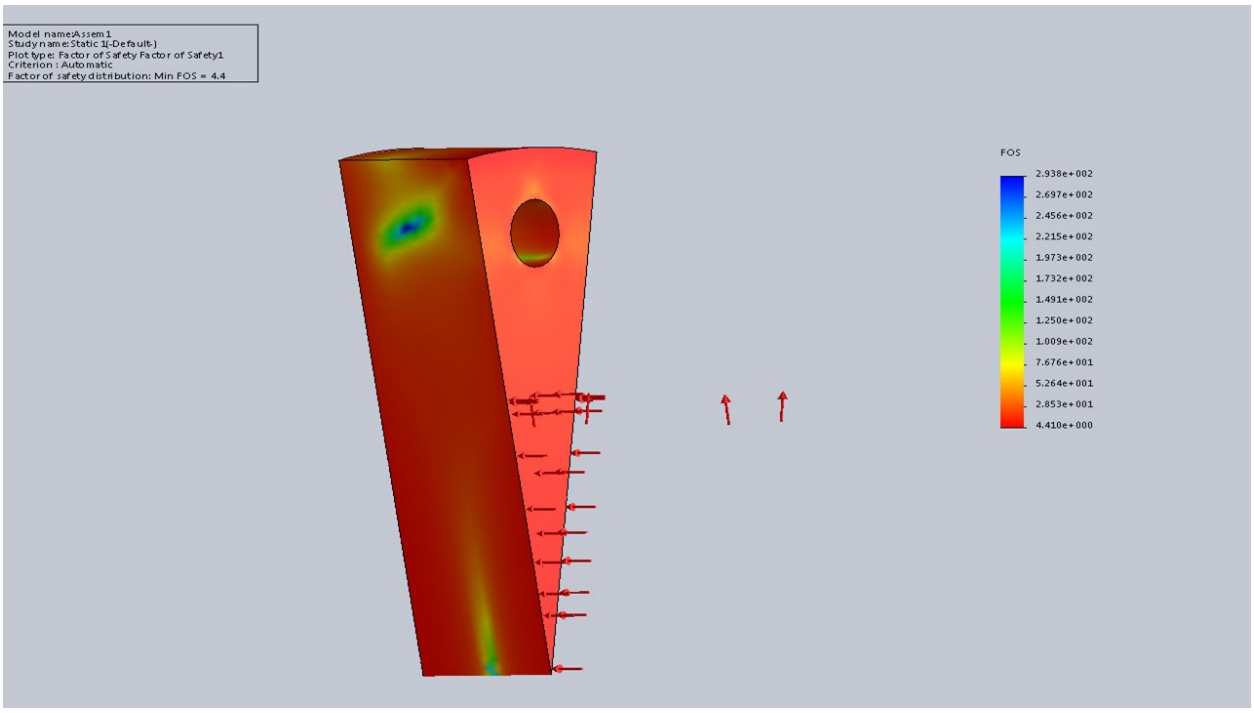

Figure 2.1.5: FEA simulation of Driver blank at 2200 psi

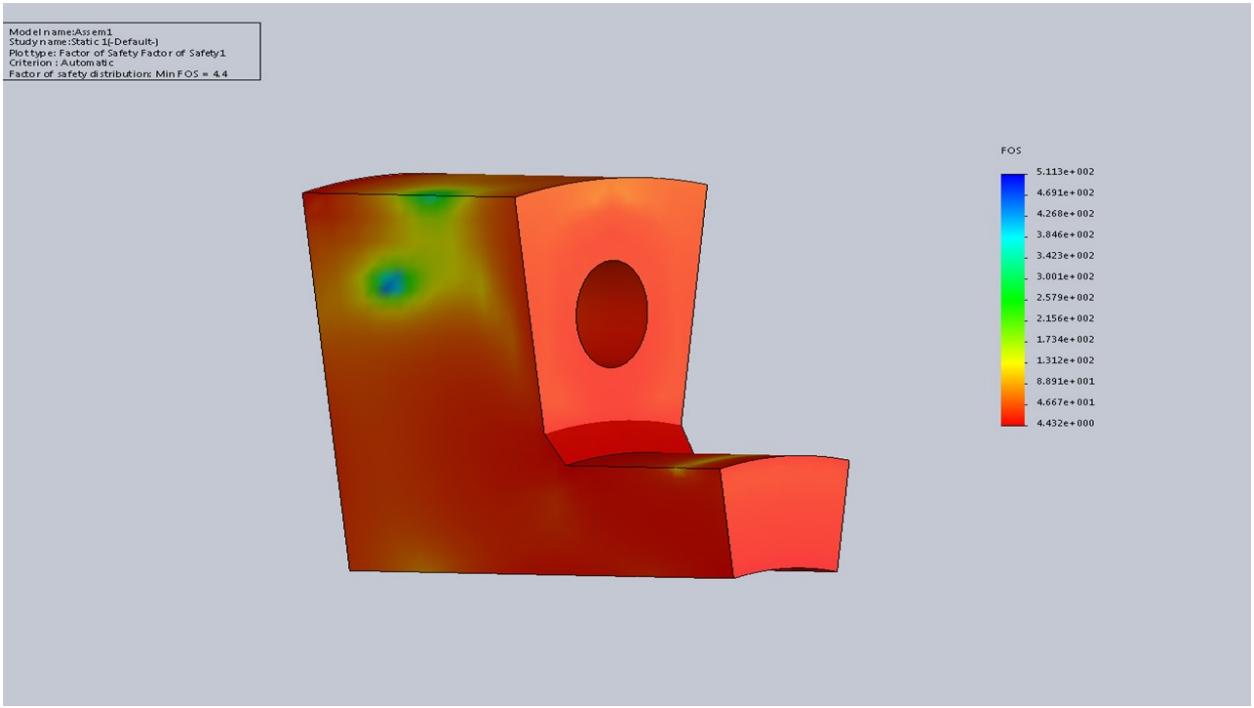

Figure 2.1.6: FEA simulation of Socket-weld flange at 2200 psi

an inside square cross section of 5.5 inches. The reason for choosing a square cross section is because the experiments require a quasi-2D condition. Additionally, a square cross section

is a practical choice to mount windows, sensors, and camera stands onto the shock tube, and makes machining easier for drilling and tapping holes. The highest pressures experienced in the driven section will be due to reshock. For a Mach 2.5 shockwave this pressure is 600 psi. The results for FEA simulations of the driven section can be seen in figure 2.1.7, for 600 psi the FOS is 2.5.

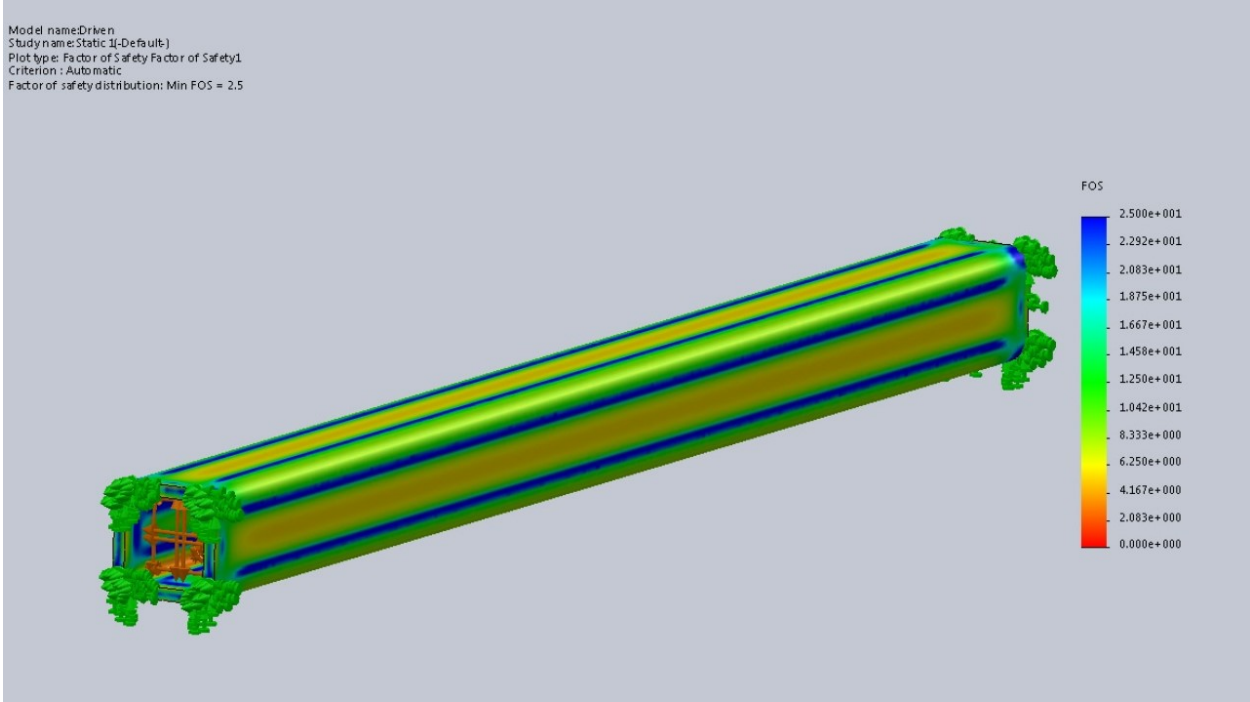

Figure 2.1.7: FEA simulation of Driven at 600 psi

The flanges attaching the driven sections together were also chosen to be made of A514 for the same reasons as those mentioned previously. Since the forces experienced in this section are much lower than in the driver section, the thickness was brought down to 1 inch. FEA analysis of the driven section indicated that for a pressure of 600 psi the factor of safety was 22.

The shape of the flanges were made in a square shape to accommodate the square cross section of the tube. Additionally, these flanges could be made from a single rectangular sheet, that can be cut into individual squares saving wasted material costs. Much like the driver, the driven flanges were made as a socket-weld type. The bolt pattern for this was a

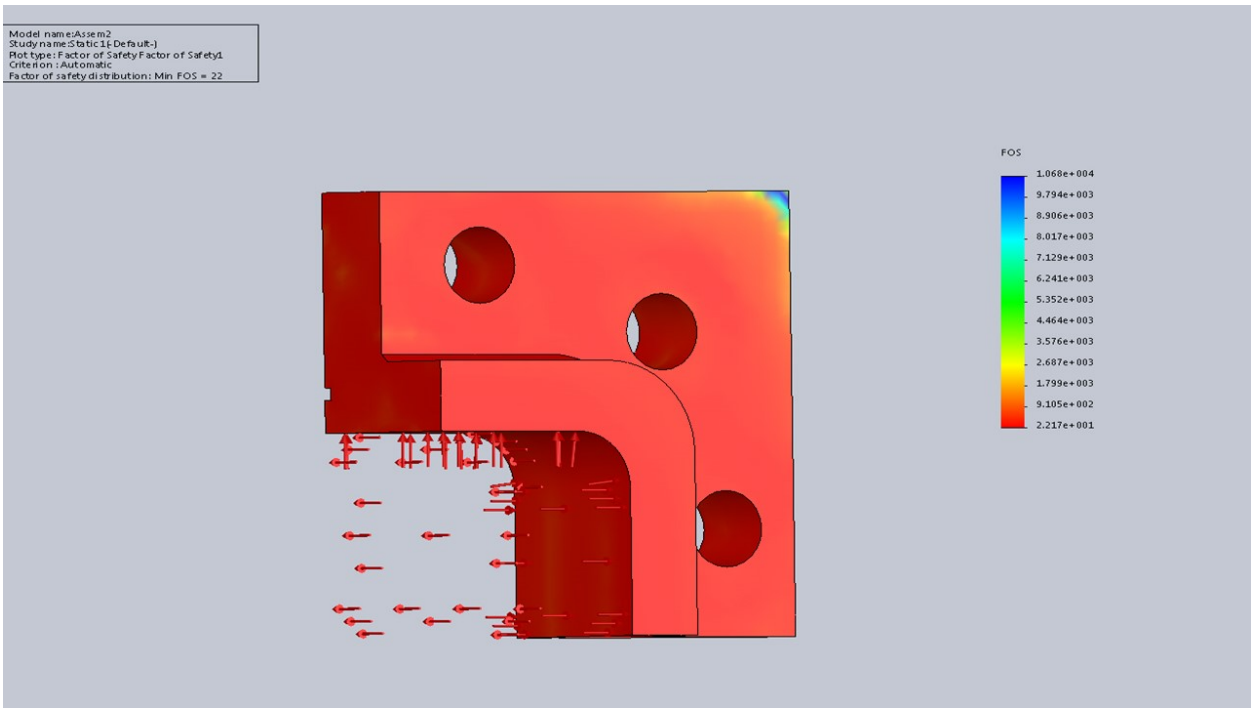

Figure 2.1.8: FEA simulation of square flange at 600 psi

bit more difficult, using an 8 bolt pattern like the one seen in figure 2.1.9a) would lead to leaking vulnerabilities at the corners, instead a 12 bolt circular pattern was used.

2.1.3 Test Section

The test section is by far the most important part of the shock tube for experiments. In this section the interface is created, shocked, and observed. Most of the post processing data is collected in the test section. The design requirements for this section is that it had to be modular enough to allow for different arrangements and test cases, whether that be different interface perturbations, orientations of the interface, or whether or not reshock is observed. There needed to be window holes that are optically transparent to view the interface at different evolutions in time. There needed to be a universal slot that would allow placement of various interface creation nozzles. Lastly, the test section had to be made sturdy enough to withstand reshock pressures that are felt. The test section is made from the same A500 square tube as the driven section, this is to ensure the shock wave remains

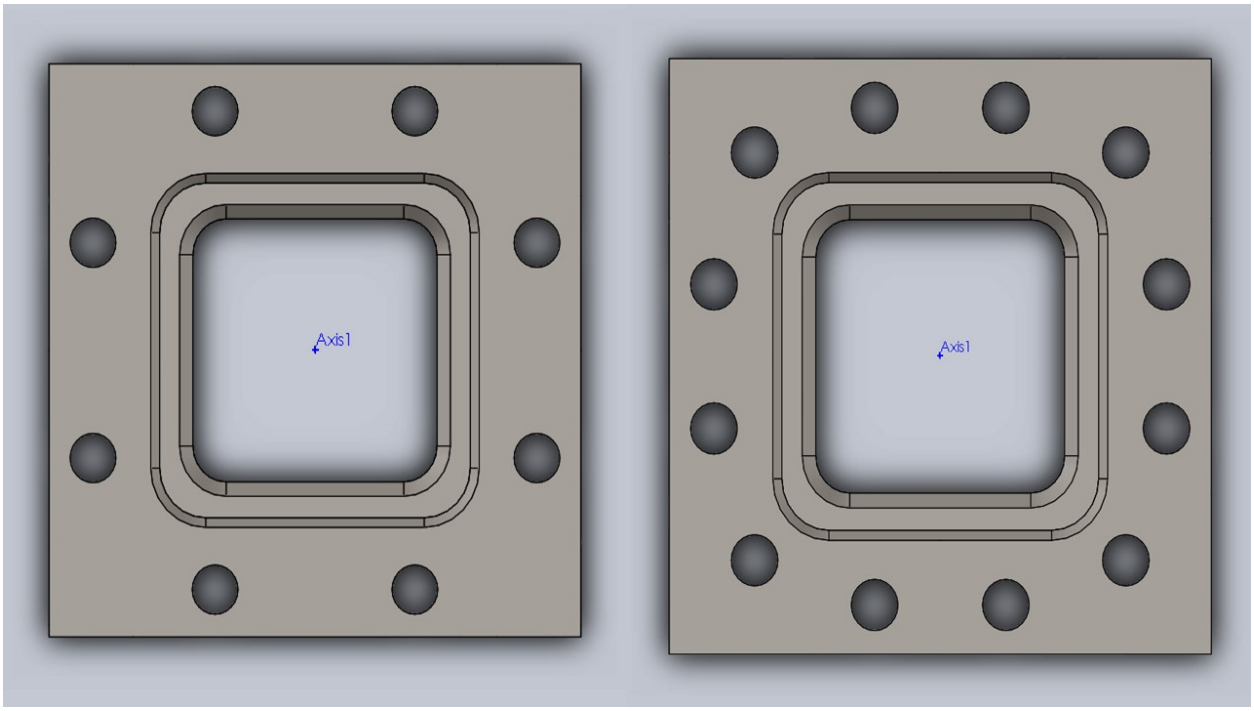

Figure 2.1.9: a) 8 bolt pattern and b) 12 bolt pattern

constant and undisturbed when transitioning from the driven section into the test section. The test section is made up of 3 sub sections, each are 3 feet in length. The sub sections are referred to as the interface creation section, run off section, and reshock section. This can be seen in figure 2.1.10. Each one of these subsections serves a particular purpose. The interface creation is responsible for creating the fluid interface. It has 5 window holes and two 1 inch wide slots for the interface pieces, one for the inlet gas and one for the exit gas. A detail of the interface creation section can be seen in figure 2.1.11. The run off section is a blank tube with no windows or slots. It acts as an extension to allow the shock wave to travel further before reflecting back upstream. The reshock section has 5 window holes for investigating reshock, additionally it can act as an extension for the shocked interface to develop into later time. Collectively these three subsections will be referred to as the test section for simplicity. The pressures experienced in this section will be much lower than the driver section. For a maximum pressure of 600 psi due to reshock, FEA simulations indicated that these sections had a factor of safety of 2.7.

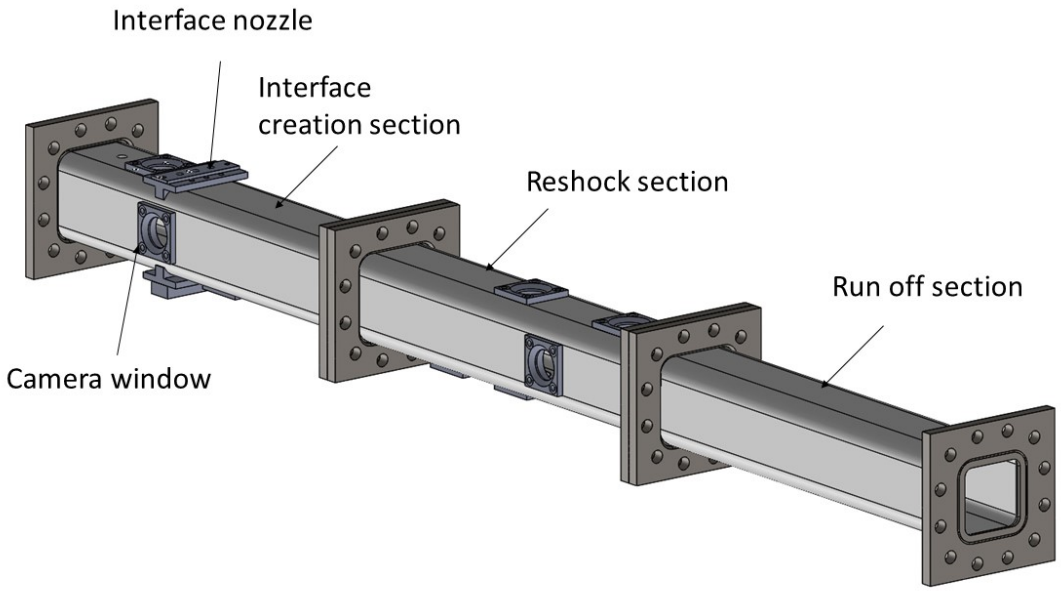

Figure 2.1.10: Test section

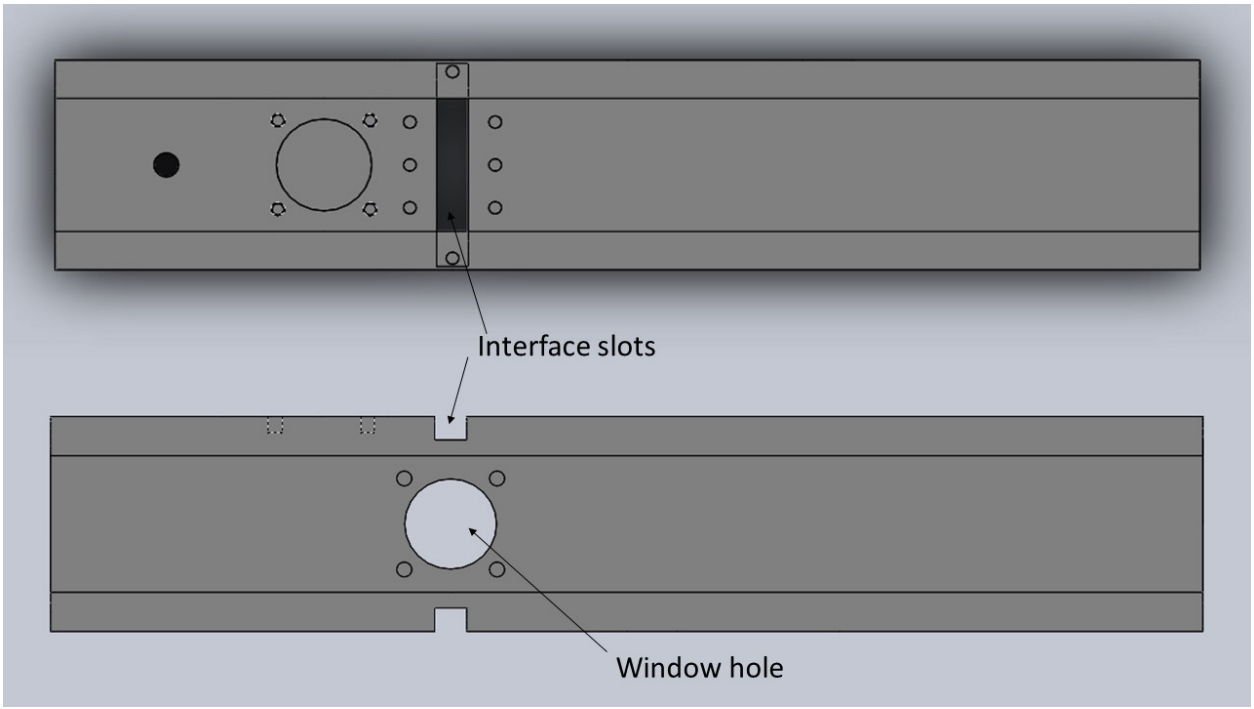

Figure 2.1.11: Detail of interface creation section

Similar to the driven section, the flanges connecting the test section were made in the same material, shape, and bolt pattern. Using this common flange pattern allows for the

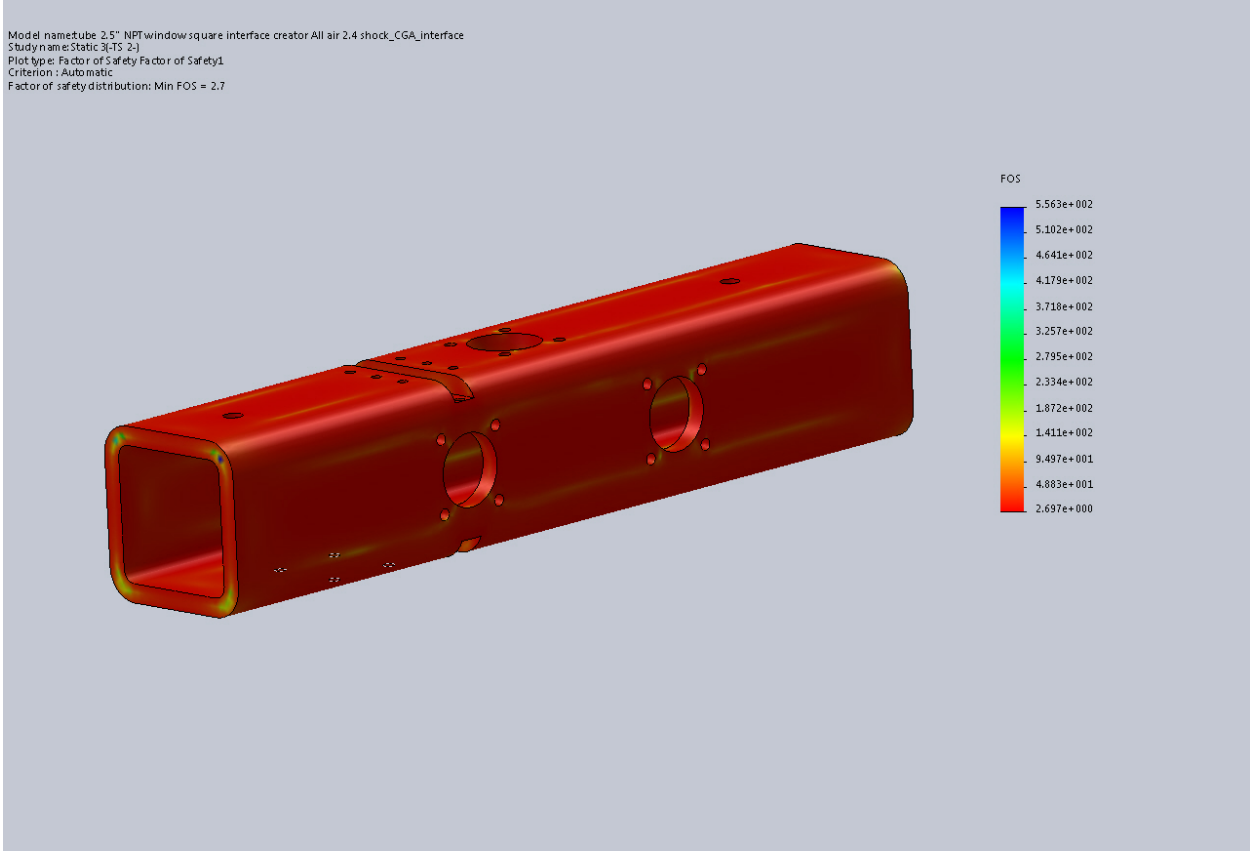

Figure 2.1.12: FEA simulation of test section at 600 psi

pieces to be interchanged within a location of the shock tube increasing its versatility. At the very end of the test section there is a blank square flange that closes it off. The pressures from this flange will experience the same 600 psi pressures as the walls of the test section. FEA simulations indicate that the factor of safety is about 11. Making it more than capable of handling the pressures experienced in reshock.

2.1.4 Bolted Connection

Once the design of the flanges were finalized, fasteners for the shock tube were investigated. Safety is the number one concern of any lab therefore using strong bolts was desirable. The bolts that would bear the most forces are the ones located at the ends of the driver and test section respectively. Using $F = P \cdot A$, the total force can be found if the pressure acting on the area is known.

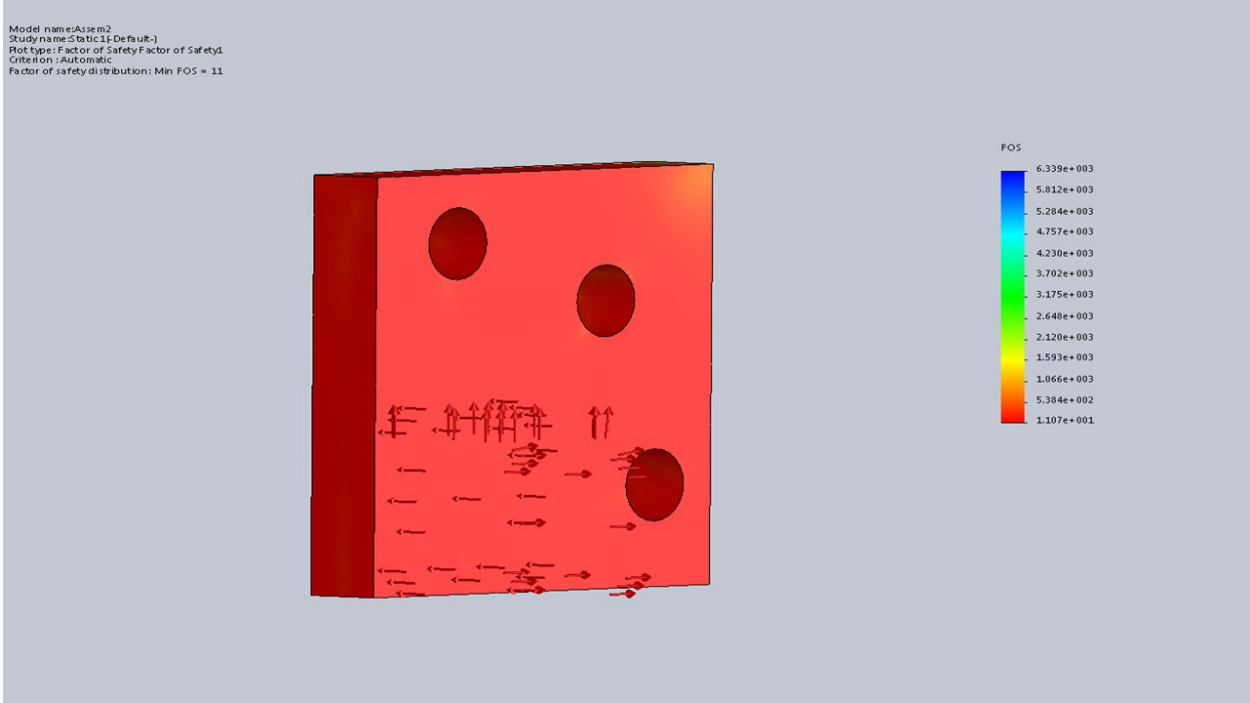

Figure 2.1.13: FEA simulation of blank flange at 600 psi

In the driver, the area in which the the pressure pushes against the blank flange is an 8.75 inch diameter circle. For a pressure of 2200 psi, the total force is 200,000 lbf. Since there are 18 bolts, each bolt will experience 1100 lbf. 1 inch Grade 8 bolts were the chosen bolts for their yield strength of 130 ksi [34]. The tensile stress area for this bolt size is .606 in^2, the axial stress on the the bolt is therefore 1815 psi. The factor of safety of these bolts is 71 making them capable of keeping the blank flange from coming off.

For the test section the area in which the pressure pushes against the blank flange is a 5.5 inch square. Using the same equations the total force exerted on the bolts is 18,150 lbf. The tensile stress area is the same, therefore, the axial stress acting on the bolts located on the blank flange are 2495 psi per bolt, giving a factor of safety of 52, which is a high enough safety factor to ensure the shock tube is safe.

2.1.5 Diaphragm Loader Design

The diaphragm is located between the driver and driven sections of the shock tube. Here is where the pressure differential is established. As the driver is put under pressure the diaphragm begins to bow out like a bubble, at a specific pressure this diaphragm will break releasing compression waves that develop into shock waves. A picture of a diaphragm before and after an experiment can be seen in figure 2.1.14

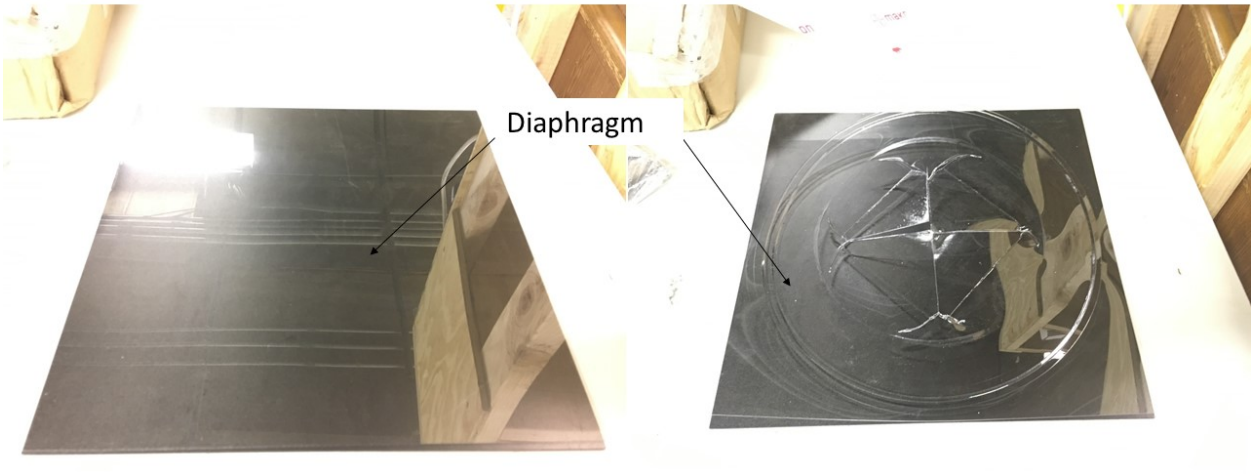

Figure 2.1.14: Diaphragm before experiment (left) after experiment (right)

Since the shock tube would be run constantly during the day a quick and easy diaphragm loader was needed. The flange face of the diaphragm loader was to be machined with a CNC to ensure the peaks and troughs would clamp down on the diaphragm to keep it from moving around. A solid works model can be seen in figure 2.1.15.

Since the driver is a circular tube and the driven is a square tube there needed to be a transition from circular cross section to square cross section. This is where the cross section change (CSC) flange comes into play, seen in figure 2.1.16. The CSC has the same peaks and troughs as the diaphragm flange but they are machined to be male. The male parts fit into

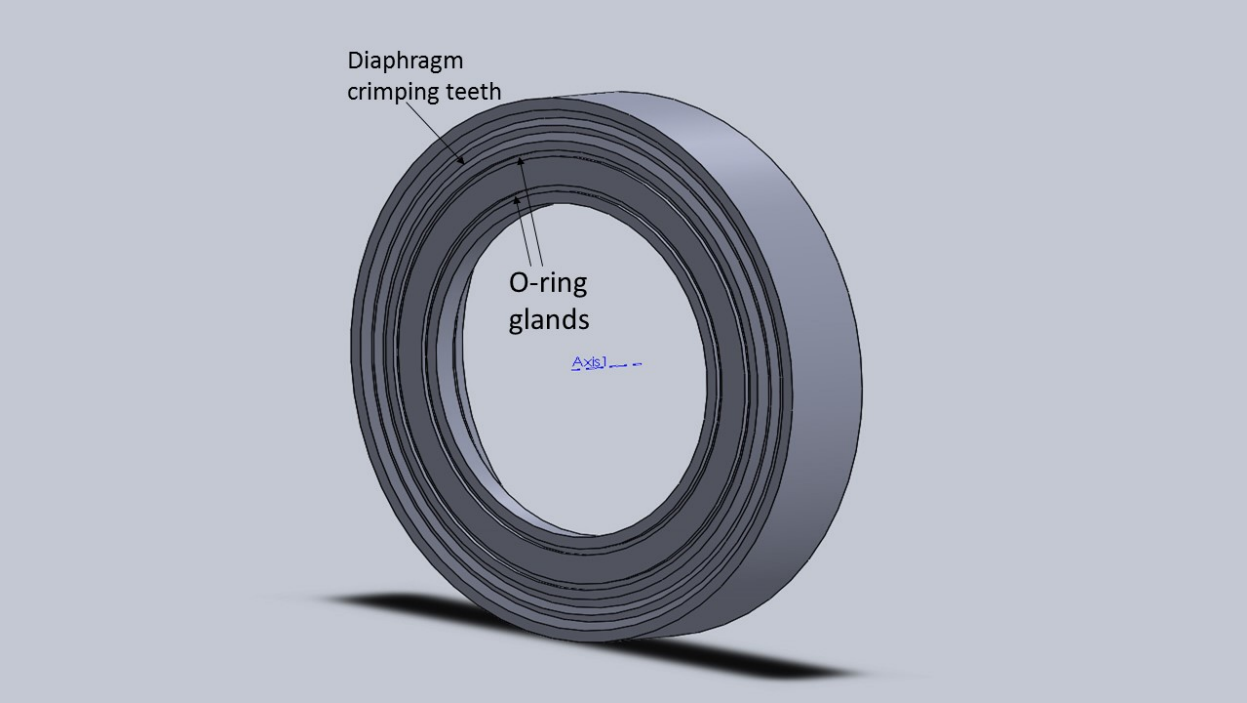

Figure 2.1.15: SolidWorks model of diaphragm flange

the peak and troughs of the diaphragm flange essentially creating a crimp between the two mating surfaces. The notches on the fillet corners are for the knife edge to sit into the CSC flange. The knife edge design would allow for an even, repeatable rupture of a diaphragm at high pressure.

The loader is simple, two "C" clamps attached to a half moon piece on one end and a store bought hydraulic ram on the other side are put together to form one half of a two piece diaphragm loader system. The low profile rams are connected to a commercially available air powered floor jack that can output up to 10,000 psi. The diaphragm loader fits between the diaphragm flange and the CSC flange sandwiching the two together. When the pump is activated the hydraulic rams push out at 10 ksi each, clamps down the flanges and keeps them from separating. The design allows for a quick reload of diaphragms since most shock tubes use bolted connections which take a long time to remove and re-tighten. This design is limited however to lower Mach numbers. Since the 4 hydraulic rams can only clamp at a maximum of 40,000 lbf the diaphragm loader is limited to a pressure of 660 psi in the driver,

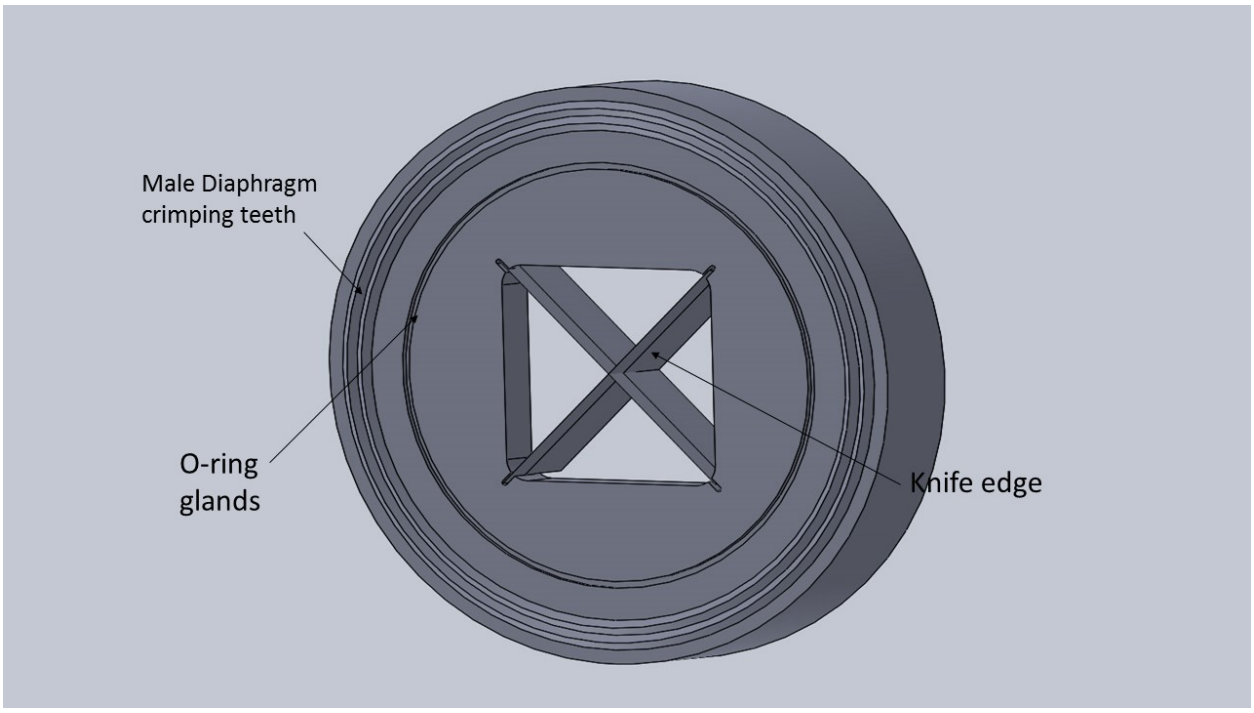

Figure 2.1.16: SolidWorks model of CSC flange

corresponding to a Mach 2.0 shock wave.

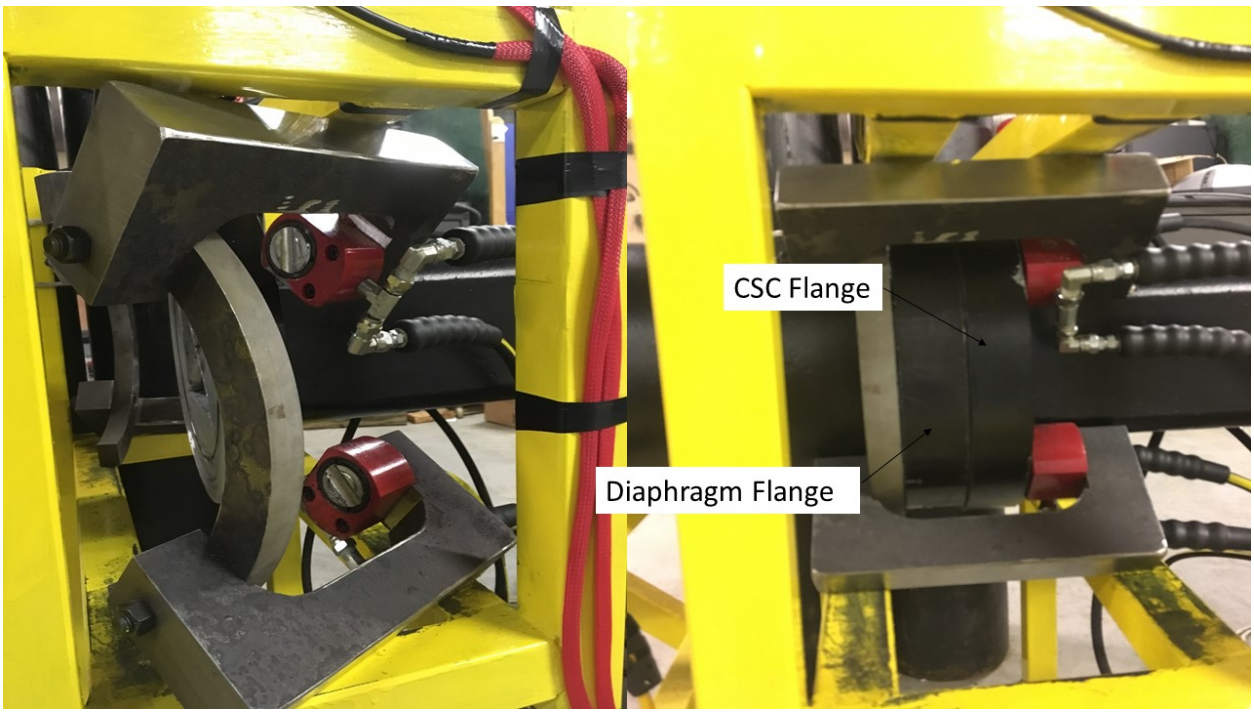

Figure 2.1.17: Diaphragm loader disassembled (left) assembled (right)

2.2 Density Gradient

2.2.1 Interface Pieces

The perturbation of the interface is achieved by a nozzle of geometric shape to create the interface. In this study a single gas cylinder is used. This can be seen in figure 1.3.9. Here, a single column of particle seeded gas is injected into the shock tube test section, this view is from the side of the shock tube where the axis of the gas column is parallel to the plane of the shock wave, this will be referred to as the vertical plane. Another view of the gas column is the center plane. Here the gas column is viewed from the top down.

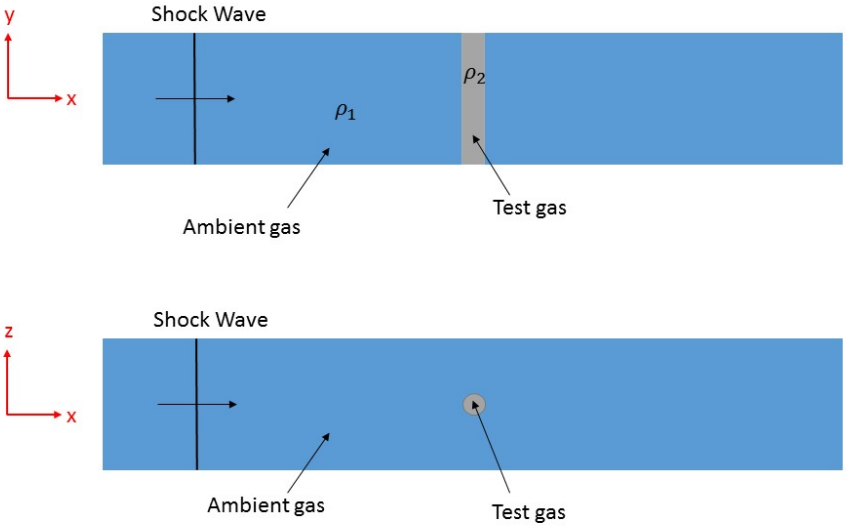

Figure 2.2.1: Gas Cylinder as viewed from the Vertical Plane (top) and the Center Plane (bottom).

The interface slots in the test section are made in such a way that different perturbations can be created in the shock tube. The one studied in this paper focuses on a gas cylinder shape as seen in figure 2.2.3. The interface pieces consists of two parts, there is the jacket gas piece and the test gas piece. The jacket gas pieces fits over the slot and the test gas is bolted down onto the jacket gas piece. This creates and annular co-flow interface perturbation. The

reason fo this co-flow design is to prevent Kelvin-Helmholtz instabilities from developing in the test gas. The factor of safety of the interface piece is 5.6 making it capable of withstanding the pressures experienced in reshock.

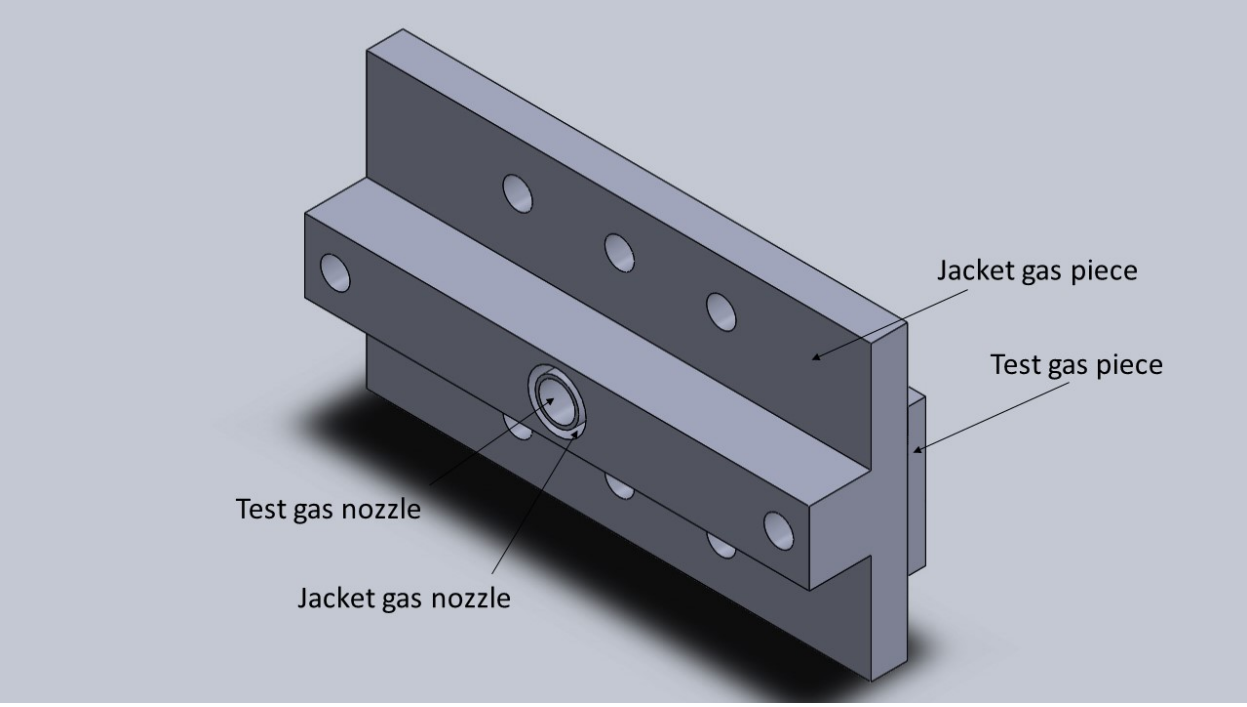

Figure 2.2.2: gas cylinder interface nozzle

2.2.2 Particle Delivery system

Adding particles, measuring their size, and the amount being injected in an experiment was the task of another graduate student's work, currently this students work is still in preparation and will not be submitted until after this thesis has been accepted. Adding particles in the shock tube is an important aspect of the entire design of the facility since without it there is no experiment. The particles here have two roles, they are used as a tracking mechanism for the shocked interface, but they also serve as a means to increase the effective Atwood number. A particle delivery system (PDS) is needed to achieve this. It was constructed out of a 35 gallon plastic water tank. Inside the tank are 6 APC 1.65 MHz nebulizer boards that are enclosed in a water tight aluminum boxes. Ultrasound is known to

atomize liquids using Faraday excitation [35], the ultrasound waves from the device radiates through the liquid and water particles separate from the surface. The results is a fog of water particles. The particles however do not move around much inside the water tank therefore a long tube extends to just above the surface of the water to allow particles to travel into test section. Finally two taped holes are drilled into the water tank, one for the gas inlet and one for the gas outlet. The flow rate is controlled using Aalborg digital flow meters. The outlet comes out a small hose directly in to the test gas interface piece. Each nebulizer is capable of creating 350cc of water particles per hour. The way to measure particle size is by using interferometry techniques. When a laser sheet of known wavelength strikes a medium, such as a particle at a precise angle it will create fringes. These vertical fringes can then be captured on a camera. By measuring the number of fringes and knowing the wave length of the light, the particle size can be determined. It should be noted that the nebulizers used in this study create a distribution of particles sizes. The objective of the student's work was to capture enough particles to determine the mean diameter of the particle using a histogram, seen in figure 2.2.4. From the study it was found that the mean size of the particles were around 2 microns.

2.3 Instrumentation, Control, and Visualization

2.3.1 Dynamic Pressure Transducers

There are two ways of knowing the speed of a shock wave. The first way is to use equations 1.2.7 and 1.2.11. This is the calculated method since it uses the diaphragm pressure ratio to predict the Mach number and wave speed. However, experimental conditions are not always ideal; the theoretical calculated wave speed is not always the same as the measured wave speed in experiments. Knowing exactly what the wave speed is helps to determine if the camera and laser timing is adjusted correctly. The use of dynamic pressure transducers (DPT) allows for the accurate measurement of the shock wave speed. The DPTs have a second function as well, they measure the post shock pressure, p_2. This information is useful

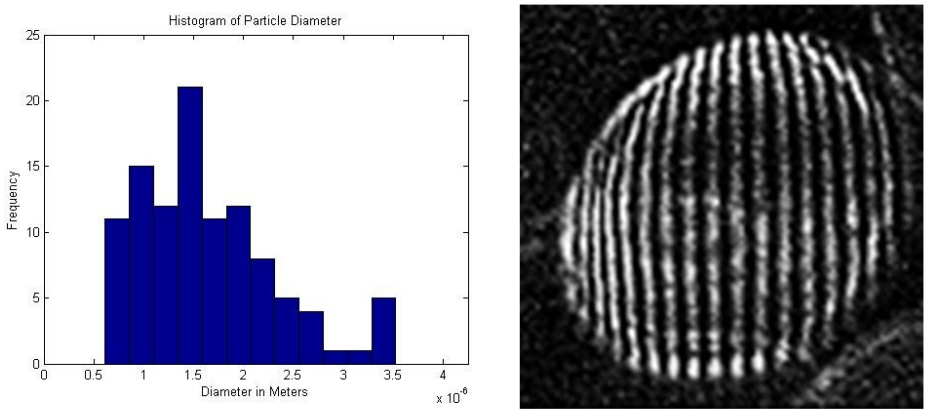

Figure 2.2.3: Particle distribution created in nebulizers (left) and interferogram of a single particle (right)

since it indicates if the experimental shock strength, $\frac{p_2}{p_1}$, corresponds to the calculated shock strength from equation 1.2.7. To measure the wave speed there needs to be at least two DPTs separated some known distance, when the shock wave passes the first DPT, it will be triggered followed shortly by the second DPT downstream. The elapsed time between the two triggers is Δt. If the distance between the two DPTs is known, in this case 4 inches from center to center, the wave speed can be calculated using $x/\Delta t$. The DPTs used in this facility were PCB Piezotronics 113B series. They use a capacitive type measuring which allows it to read pressure changes at extremely high rates. The nature of capacitive type devices means their signal decays with time making them capable of reading only dynamic changes in pressure not static changes. These DPTs are capable of measuring shock data at a sampling rate of 2MHz. They are connected to a signal conditioning device which is used to convert the signal into a voltage and using a scale factor the voltage can be converted to pressure. Once the shock speed is determined the necessary camera delays can be calculated and implemented in Insight 4G to take images of the interface. The driven section has

several 3/4 inch NPT holes. When they are in use for DPTs, custom made 3/4 NPT fittings are inserted. When the holes are not in use they can be plugged up with a commercially available 3/4 NPT plugs as seen in figure 2.3.1.

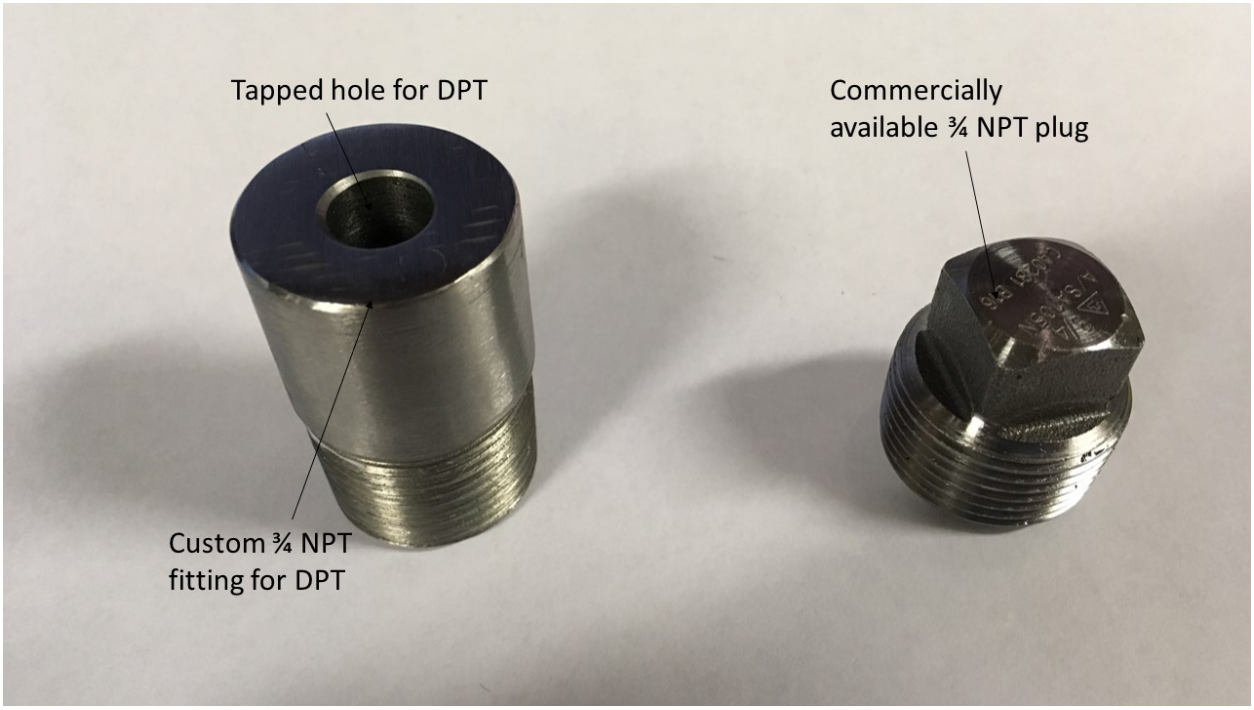

Figure 2.3.1: Custom made fitting for DPT and commercially available NPT plug

2.3.2 Control Valve System

For experiments, various parts of the shock tube will be filled with gas. The driven and test section for example are filled with air or nitrogen gas, the driver is filled with nitrogen or helium gas at higher pressures. A plumbing system is needed to be incorporated to the shock tube to allow for a systematic and organized way to fill parts of the shock tube. As stated in the previous section, the driven section has several 3/4 NPT tapped holes, in addition to being the locations of the pressure transducers they also serve the purpose to mount hoses for the delivery of the upstream gas. The test section blank flange also has a tapped hole for delivery of the down stream gas. The hoses are opened and closed using solenoid valves that can be operated at the control center. The driver section has a tapped hole in the

blank flange, the solenoid use here is rated to pressures of up to 2200 psi. A figure of the gas delivery system can be seen in figure 2.3.2.

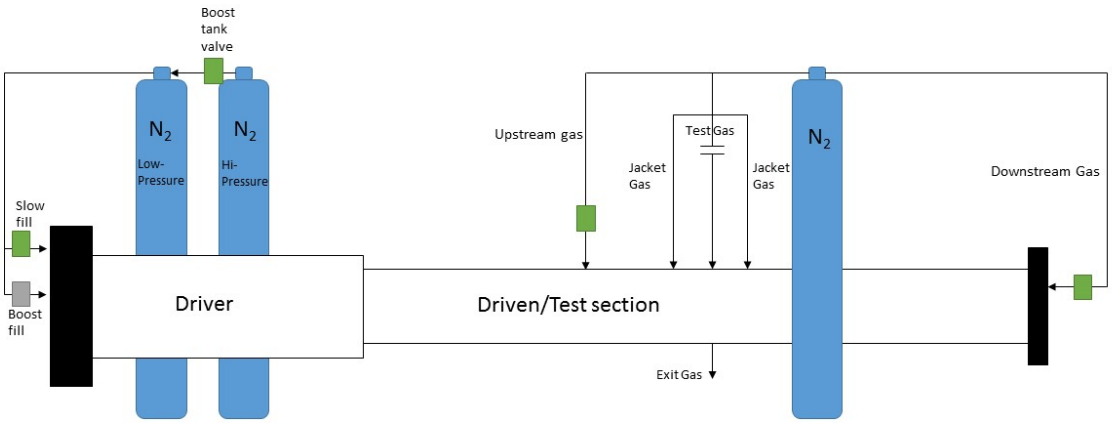

Figure 2.3.2: Gas delivery system

The way in which the gas delivery system requires some explanation. A single bottle fills up the driven and test section with nitrogen gas. The hoses that fill are labeled "upstream" and "downstream" gas. As gas fills this section it forces air to come out of the bottom of the shock tube. Meanwhile the same bottle also supplies gas through the particle delivery system, which carries water particles seeded into nitrogen gas and to the test section, this is represented by the broken line. The particle seeded gas is then injected into the test section labeled "Test gas". The jacket gas is branched off from a "T" bypassing the Particle delivery system and straight into the jacket gas nozzle. The plumbing system for the driver requires a bit of explanation. There are two gas bottles that are used in this system, in the figure they are labeled "Hi-Pressure" and "Low-Pressure". In the setup the high pressure bottle when completely filled is 2200 psi. This bottle feeds gas into the low pressure bottle, the idea is to keep the low pressure bottle at approximately 500-600 psi during experiments. As

the high pressure bottle reaches equilibrium with the low pressure bottle it is discarded and replaced with a full bottle at 2200 psi. The low pressure bottle is the primary means to fill the driver. It is connected to two different solenoids, a "slow fill" and a "boost fill". The slow fill solenoid is the one that gradually fills the driver with gas, while maintaining 500 psi in the low pressure bottle, this is all maintained at the control center. Once a target pressure is reached the slow fill valve closes. The boost valve is then activated, it fully opens and allows a rapid amount of gas to enter the driver and provides the instantaneous amount of dynamic pressure needed to rupture the diaphragm and fire a shock wave. The boost valve opening time can be adjusted depending on the experiments, but usually 500 ms is enough boost pressure to rupture the diaphragm

2.3.3 Control and Measurement system

Having a control and measurement system is key to running experiments efficiently. The system allows the operator to fire shock waves, record data, and trigger the optical devices at precise moments in time. Before sophisticated systems were invented shock tube experiments relied on the operator to make careful adjustments to the shock tube every time they were run [36, 37]. The system incorporated in the facility also has a second purpose, it serves as a means of communicating the hardware and software. All of the hardware in the system is managed by a National Instruments PXIe-1073 chassis with a PXIe-6356 Multi function DAQ and a PXI-6229 Multifunction DAQ. For the purposes of simplicity the PXIe-6356 will be referred to as the "Fast card" and the PXI-6229 will be referred to as the "Slow Card". The fast card is capable of measuring 8 simultaneous Analogue input channels at a rate of 1.25 million samples per second. The slow card is capable of measuring 16 simultaneous channels at a rate of 250 thousand samples per second. The slow card is used mainly for the gas delivery system, whereas the fast card is used for the DPTs and Laser/Camera system. The DPTs are used for triggering the optical hardware by first triggering one of the built in counter timers in the NI hardware. The timers then precisely trigger the laser and camera

system. These devices need instantaneous response times to capture the interface at precise moments in time. The program used is NI's LabVIEW. The program used in this shock tube facility is similar to the program that was originally used in the Texas A&M (TAMU) shock tube. Developed by Dr. McFarland and Adam Hartzell [22], this program was modified and adjusted to accommodate the needs of the Mizzou Shock Tube Lab. For example the TAMU shock tube used a single card multi function DAQ to control all of the functions of the shock tube, including the fast response devices. Since the Mizzou shock tube separates the two, the code in LabVIEW had to be modified such that the analogue inputs from the DPTs would be read and processed in LabVIEW.

2.3.4 Window Design

The windows are an important aspect of the shock tube, they are the means to view the interface developing at different stages of the experiment. The windows had to be removable since the shock tube emphasizes a modular design. They needed to be optically transparent in the visible region since the light scattered from the water particles was 532 nm. The windows need to be robust enough to withstand the pressures that are experienced post shock, and they need to be inexpensive to make, so that the construction can stay within budget. The size of the windows is limited to the width of the flat portion of the shock tube walls between the fillet corners. This means the windows have to be less than a width of 4.35 inches. The holes for the window cover are 3 inches in diameter with four, 7/16" female threads machined on each corner of the quadrants of the circle spaced 1.45 inches from the holes center. A machined wall of the test section with the window holes can be seen in figure 2.3.2.

The interior surface of the windows have to be flush with the ID of the shock tube walls. This is to avoid any disturbances to the shock wave traveling down the test section. The windows are made from 6061 T-6 aluminum. When compared to steel, aluminum is lighter and easier to machine bringing down machining costs, since there are 11 window holes in

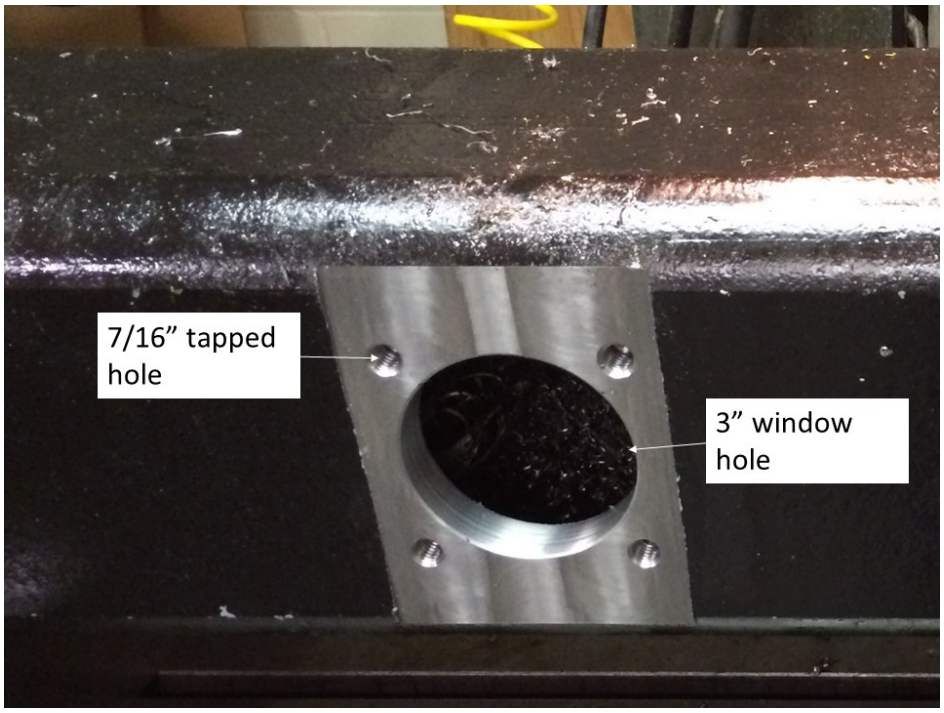

Figure 2.3.3: Machined surface of TS with window hole

the test section manufacturing costs had to be kept to a minimum. The window uses a simple flange type design. On the back of the window cover is a 3 inch OD and 2.79 inch ID cylindrical cover where the window will sit inside. On the bottom of it there is a 0.1 inch thick lip that has a gasket between the window and window cover to reduce stress concentrations on the plastic window.

The transparent window material used was made of clear acrylic plastic. When compared to polycarbonate, acrylic is less expensive than polycarbonate. Acrylic also has better light transmittance over polycarbonate, and it is scratch resistant. Furthermore, it can be polished whereas polycarbonate cannot. The design of the complete window can be seen in the solid works model on figure 2.3.4.

The aluminum window cover has four bolt holes where grade 5, 7/16 inch bolts are fastened down. From reshock pressures of 600 psi, the force acting on each of the bolts is 1060 lbf. The axial stress on a single bolt is 4141 psi. Grade 5 bolts have a yield strength 92 ksi, The FoS is therefore 22. Making these bolts capable of keeping the window from coming

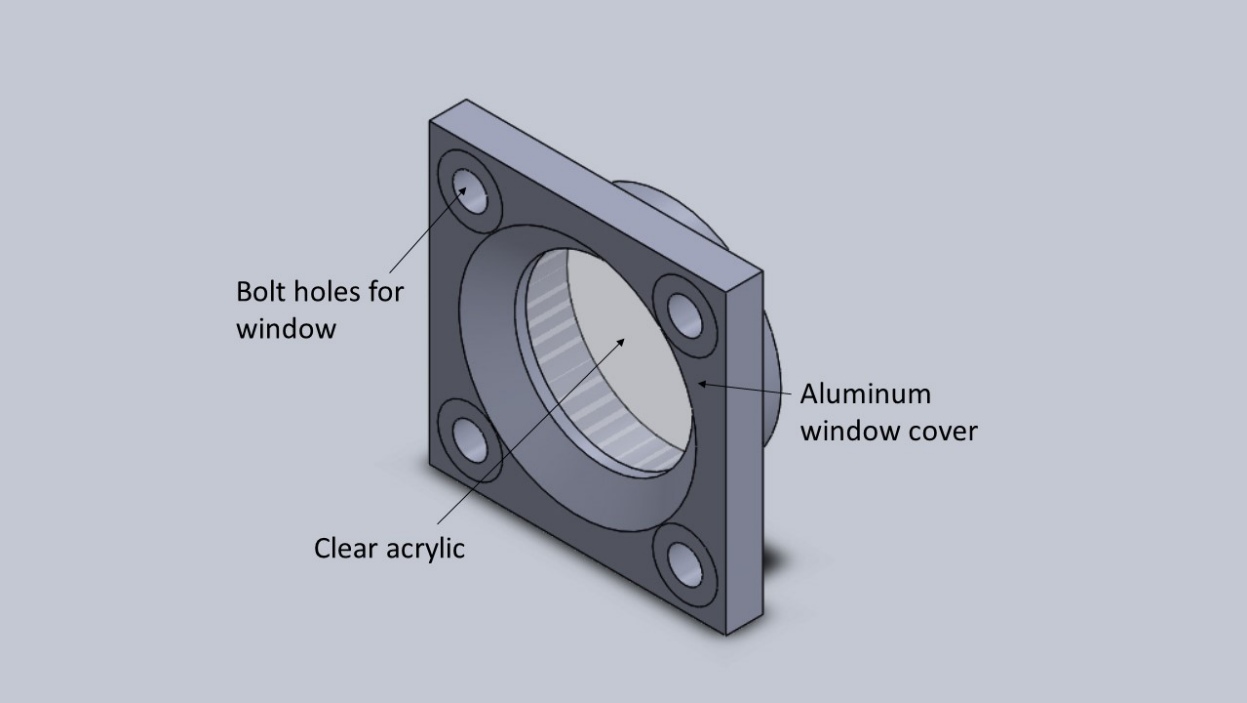

Figure 2.3.4: SolidWorks model of window assembly

off of the shock tube. The choice to use a circular shape for the acrylic window was to avoid stress concentrations at the corners of the window which would be a weak point in the design. They are made from 3/4 inch thick acrylic sheets that were cut to the desired disk shaped size. Initially it was proposed to use laser cutting, but it was found that this method results in small burrs at the edges of the cut. Water jet cutting was the chosen fabrication method since it produces a cleaner cut along the edges minimizing fabrication costs. This method proved to be the most cost effective method since it did not require extensive machining and polishing of the acrylic, the sheet used in fabrication had a protective film cover that could peel off once the machining was finished. Furthermore, the thickness was uniform on all the pieces since the acrylic originated from a single extruded sheet. The windows are located in the test section, therefore, they will experience 600 psi of pressure due to reshock. Using SolidWorks simulations the acrylic windows have a FOS of 2.8 which will allow the windows to withstand the pressures that are experienced in the shock tube during reshock. The aluminum pieces have a FOS of 2.0 showing that they will too withstand the pressures

in reshock.

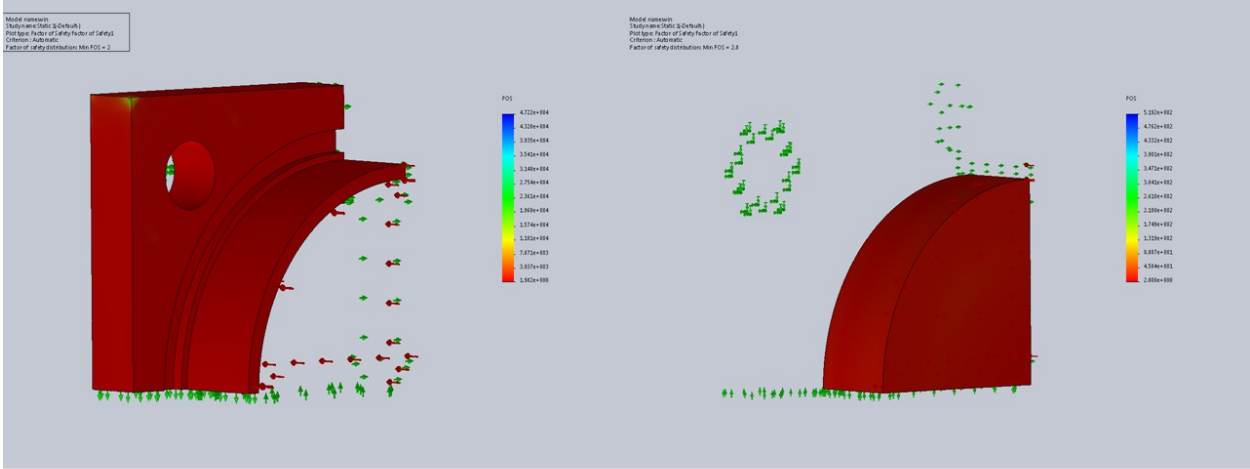

Figure 2.3.5: FEA of window cover at 600 psi (left) and acrylic window (right)

2.3.5 Laser and Camera

Laser based optics are commonly used in hydrodynamic experiments to illuminate the particles seeded into the gas and observe the the evolution of the instability. There are two methods of visualizing the interface in a shock tube. One method is using planar laser mie scattering (PLMS) and planar laser induced fluorescence (PLIF). Mie scattering techniques can be used for particle imaging velocimetry (PIV). PLIF works by light of specific wavelength interacting with a molecule. This excites the molecule's electron to a higher state, when the electron returns to its lower state in releases energy in the form of light of longer wave length. The fluorescence depends on the wavelength of the light interacting with the molecule and the molecule's chemical properties.

The Mie scattering effect occurs when incident light interacts with spherical particles and is scattered in various directions. In theory, any particle can create the Mie scattering

effect assuming it has a different refractive index of the gas surrounding it. It is used for visualizing the interface by mixing the water particles with nitrogen or air. For this study the Nd:YAG laser set at 532 nm light was used to illuminate the water particles.

PIV uses the illuminated particles taken at two different points in time and calculates a velocity field. To understand this method, take a single particle and follow its path from one frame to the next. The displacement vector can calculated assuming you know the coordinates the particle in the first frame and second frame. If the camera straddling time is know then the velocity of that single particle can be calculated. This method is known as a particle tracking velocimetry (PTV) and uses the Lagrangian approach. In the case of PIV there are too many particles for them to be distinguished. Instead, a pattern is outlined using statistical analysis from the first frame and correlated to similar patterns in the second frame, this uses an Eulerian approach.

Illuminating the particles is achieved using a Litron Nd:YAG PIV laser. A single YAG crystal rod is surrounded by flash lamps around the circumference and semi permeable mirrors at the rod ends. The lamps "pump" energy to the crystal. Once an optimal amount of light has been absorbed by the crystal, it begins emitting light towards the mirrors, these mirrors bounce light back to the crystal rod and more light is absorbed. Once a threshold is achieved in the crystal, energy in the form of light penetrates the mirror and is directed out to the processing site. The laser beam is ejected out of the laser head and using a series of optical lenses, the beam is manipulated to a specific shape. An example of this is seen in figure 2.3.6.

The camera is the device that will capture the instability developing at a specified moment in time. The laser, camera, and program that controls the two form the complete PIV system. The PIV system consists of two TSI cameras that have an Intensified Charged Couple Device (ICCD). The cameras in this lab are 4 megapixels and 29 megapixels respectively that are arranged around the shock tube's windows. The cameras have a low frame straddling time that is used in PIV. The camera's shutter is not fast enough to open and close in the time

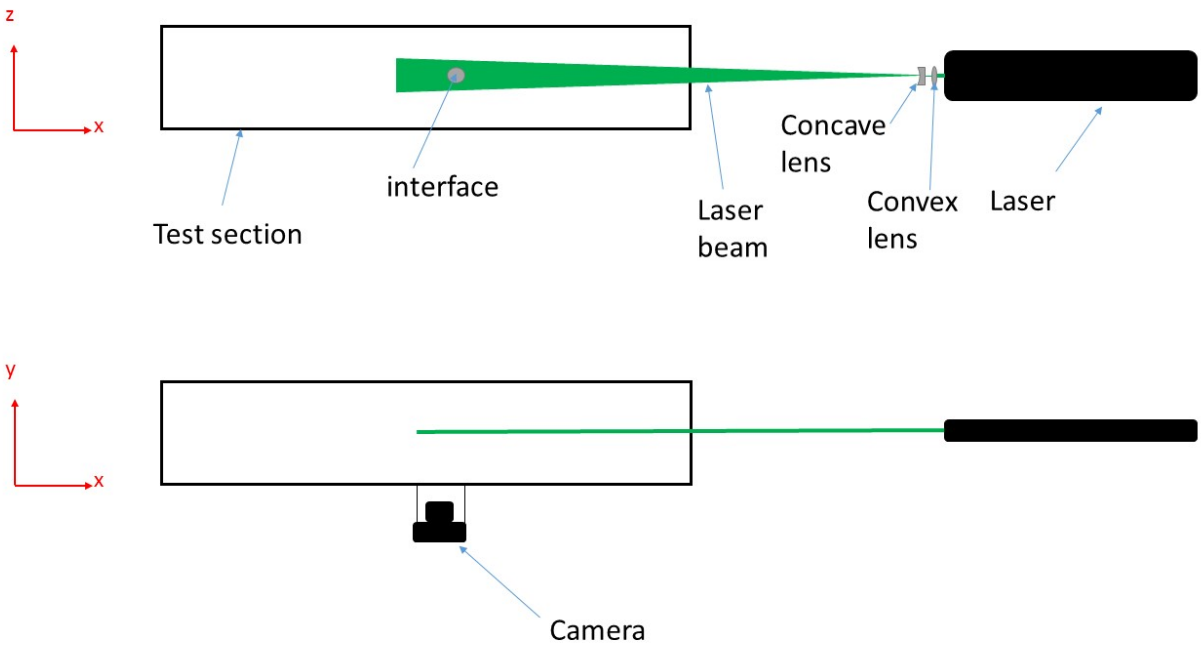

Figure 2.3.6: Diagram of laser setup

between successive pictures, instead the camera shutter remains open between successive laser pulses and the ICCD will only capture an image when the laser is fired. Various macro lenses are used in combination with extension tubes to focus on the interface. Oftentimes the camera needs to be far away from the window to focus on a larger area, similarly there are times where the camera has to be less than an inch away from the window to capture as many details of the interface as possible. The cameras are attached to custom mounts and the mounts are bolted on the windows. There are many advantages to this design over a tripod. First, the mounts are robust and sturdy; there is no worry of bumping into the stand and getting the camera disoriented, secondly the camera mounts are versatile; they can be mounted at any flat surface of the test section's outer diameter, finally it allows for precise adjustment of the camera position, such as the distance and angle. The camera mounted horizontally and vertically can be seen in figures 2.3.7 and 2.3.8, respectively.

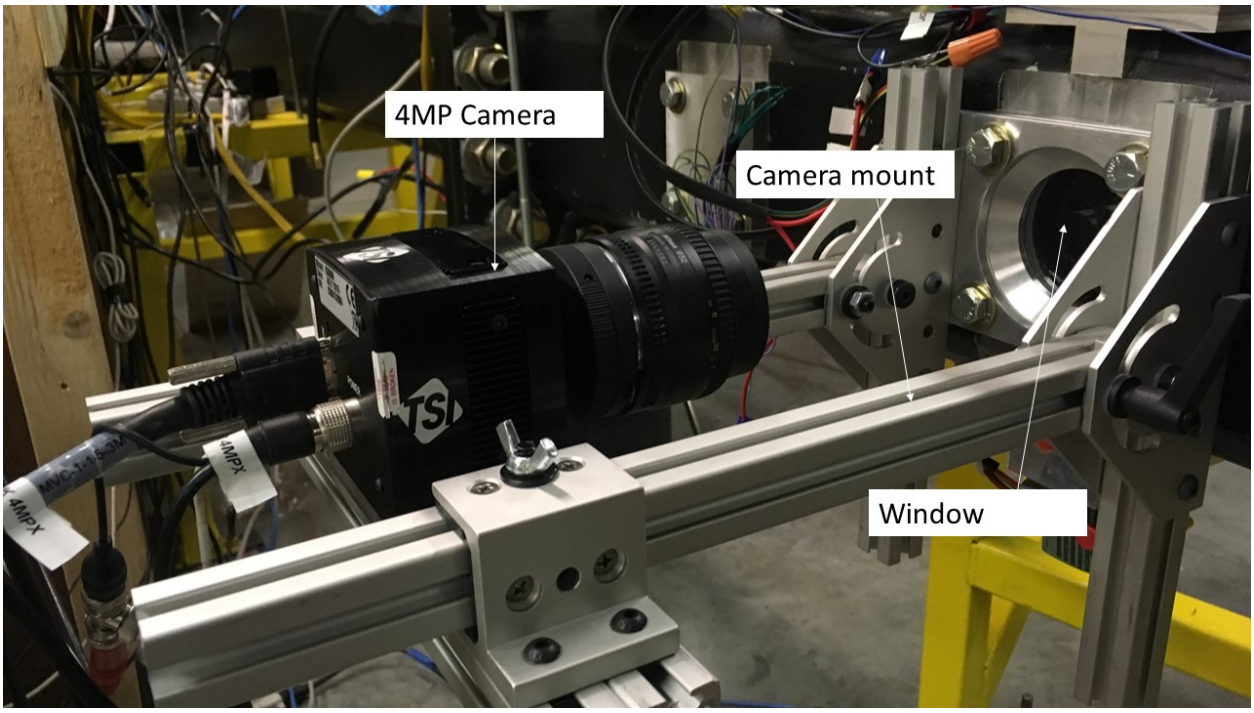

Figure 2.3.7: Camera oriented horizontally on Shock Tube

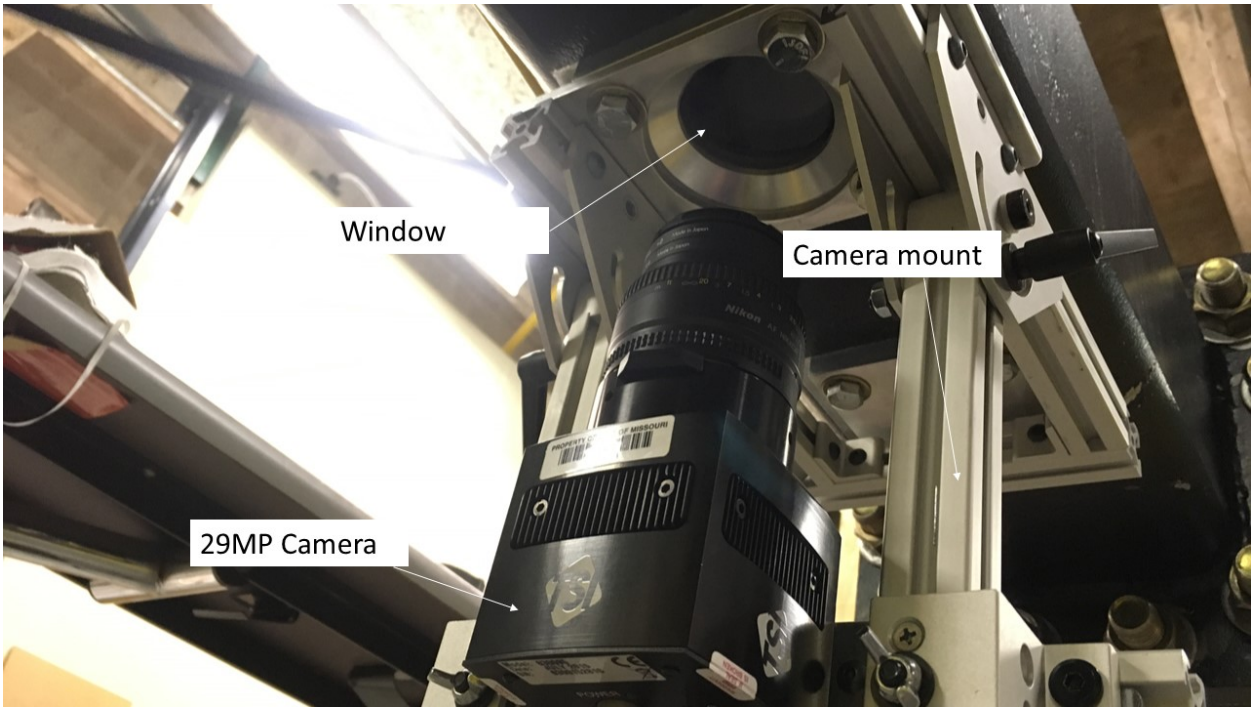

Figure 2.3.8: Camera oriented vertically on Shock Tube

2.4 Facility capabilities

The Mizzou FMSTL is a 30 foot, pressure driven shock tube, with a modular construction and interchangeable sections. The internal cross section of the driven and test section is 5.5

inches and 25 feet in length. It has an easy to remove diaphragm loader allowing for frequent experiments on a day to day basis. The shock tube weighs around 2.5 tons in total. It is bolted on stands constructed out of square tubing that are fixed to the concrete floor on grade 5 bolts. The stands have rubber shims between the ground and the legs to reduce vibrations, as well as rubber between the stands and the shock tube. It has a modular interface design which allows for various perturbations to be run depending on the type of experiment being studied. Furthermore, this facility is one of the few that runs SDMI experiments, a unique feature. The tube is designed to withstand shock strengths of up to Mach 2.5 in atmospheric air, additionally it can function with the test section blank flange attached or removed, depending on the experiments.

3 Preliminary experiments in the shock tube

This section looks at the experimental work conducted in the facility. This includes the capabilities of the facility, the experimental methods, and finally qualitative and quantitative analysis of the results. The experimental results compared are those conducted by Vorobieff [32] and simulation results obtained by Dahal [38]. The simulations performed for validation use a Particle-in-Cell (PIC) technique. This couples particles in a Lagrangian coordinate system with a fluid in an Eulerian system. This computational method was utilized in an open source hydrodynamics software FLASH.

The experimental setup consists of a particle seeded air cylinder surrounded by unseeded air. In these experiments the seeded air cylindrical column is formed by injecting air-particles though a 0.5 inch diameter nozzle at 4 LPM. For most of the experiments covered in this section an air-particle interface is investigated. In other sections however, a nitrogen-particle interface surrounded by air is used and will be discussed in section 3.4.1. The effective Atwood number for the air-particle interface is approximately 0.03 and was created using water particles droplets with a mean diameter of about 2 μm. It should be noted that

the particle size is not uniform; there is actually a distribution of particles being created of diameters larger and smaller than 2 μm. All experiments conducted in this study used a Mach number of 1.66, this resulted in an interface post-shock velocity of about 275 m/s. In these experiments, the gas conditions in the driven and test section are 98 kPa and a temperature of 293 K.

3.1 Initialization and calibration

Initial experiments of the shock tube began in the Summer of 2016. At this stage all functions of the shock tube were worked out individually and it was time to integrate them to run experiments.

The first step was to ensure the shock tube (pressure gradient) was effectively firing shock waves in a repeatable and safe manner. The shock tube was assembled and a series of dry runs were conducted. These preliminary experiments were also used to determine the absolute burst pressures of the diaphragms. In these experiments the diaphragms used were polycarbonate .030" sheets. The diaphragms burst when there is enough force pushing the diaphragm against the knife edge. For normal experiments the diaphragms burst due to dynamic pressure loading, however, for these dry runs the diaphragms would burst under static pressure loading. These dry runs would indicate what the threshold pressure was before the diaphragm sheet failed. A new diaphragm sheet is inserted into the diaphragm loader system. The shock tube is then sealed up and gas begins filling the driver. The pressure in the driver just prior to the diaphragm failing is the burst pressure for the diaphragms. For .030" polycarbonate diaphragms, the dynamic burst pressure was found to be about 100 psi. Since the initial conditions of the driven section are known, the Mach number can be calculated, in this case it is 1.66. With this knowledge the necessary adjustments could be implemented in LabVIEW to run repeatable experiments.

The next goal was to get a stable laminar jet for the interface. The interface consists of Nitrogen or air seeded with water particle droplets. The gas is injected into a water tank

where piezoelectric devices generate water droplets. The gas that enters the water tank is regulated with volumetric flow meters. The seeded gas then exits the water tank though a hose and makes its way down into the shock tube where it first passes through the gas cylinder interface nozzle and is injected into the shock tube's test section. The setup is outlined in figure 3.1.1.

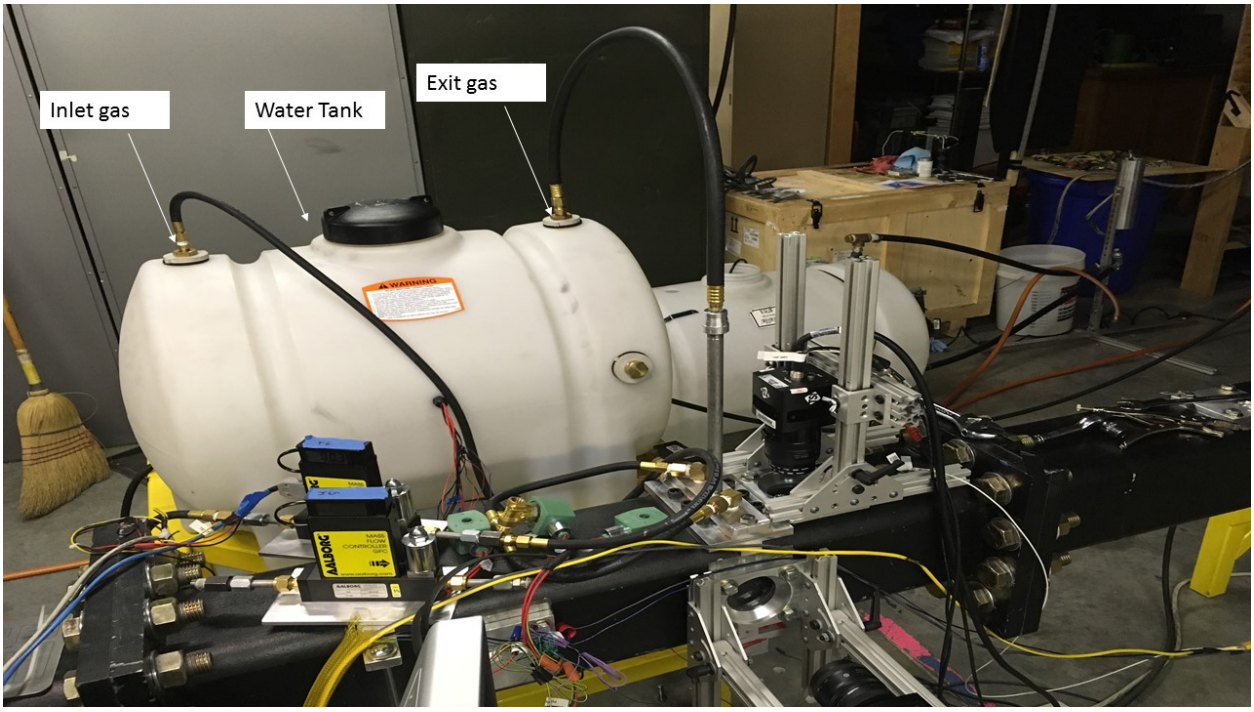

Figure 3.1.1: Diagram of interface creation system

Getting the interface to form a stable jet required some trial and error. Fluid mechanics equations provided the maximum flow rates that would create a laminar jet, however, these flow rates had to be tested out to confirm if the jet was stable. Using equation 3.1.1 the volumetric flow rate can be found, Where Q is the volumetric flow rate, D_H is the hydraulic diameter of the pipe, ν is the kinematic viscosity of the gas, and A is the pipes cross sectional area.

$$Re = \frac{QD_H}{\nu A} \tag{3.1.1}$$

For laminar flow the Reynolds number should be less than 2300. This corresponds to a

maximum volumetric flow rate of 12 liters per minute (LPM). The particle seeded gas column was then visually inspected to see if there were any instabilities forming. It was found that there is a narrow range of flow rates that would produce a laminar jet. Flow rates greater than 4 LPM resulted in unstable waves on the edges of gas cylinder resembling KH instabilities. Similarly, for flow rates less than 4 LPM the jet would break up into a distorted flow. The upstream and downstream gas that filled the shock tube provided stability in the gas cylinder. It should be noted that these flow rates had to be regulated as well. If the upstream and downstream flow rates were too large the gas cylinder would become distorted. Therefore, flow controlling orifices were used to keep the flow rates constant. Filling the shock tube with gas creates a pressure differential at the exit. This results in a gentile suction which stabilities the interface. PIV images of the interface were taken to visualize the velocity profile to ensure that it was laminar and stable. An image of the interface using PIV can be seen in figure 3.1.2. Once the initial conditions of the interface were confirmed and repeatable the next part was to get the camera and timing correctly.

The laser and camera system is the only means to visualize the interface evolving. As a result, the timing of the laser and camera had to be synchronized with great precision. If the camera took pictures too early, the shocked interface would not appear in any field of view. If the camera took pictures too late, the interface would pass from the field of view of the camera. There are two steps in getting the timing down correctly. The first step is to know when the shock wave reaches the interface, the second step is to know when the shocked interface will reach a specific camera location. Several pieces of information have to be known, the first of which is the wave speed. In these experiences for a Mach number of 1.66 the wave speed is 570 m/s. The second important piece of information is to know the distance between the triggering DPT and the initial location of the interface. With these two pieces of information, the time it takes for the shock wave to reach the interface can be easily calculated. Knowing the speed of the interface after it is shocked is the next important step in determining the camera timing. Since the windows are only 2.79 inches in diameter

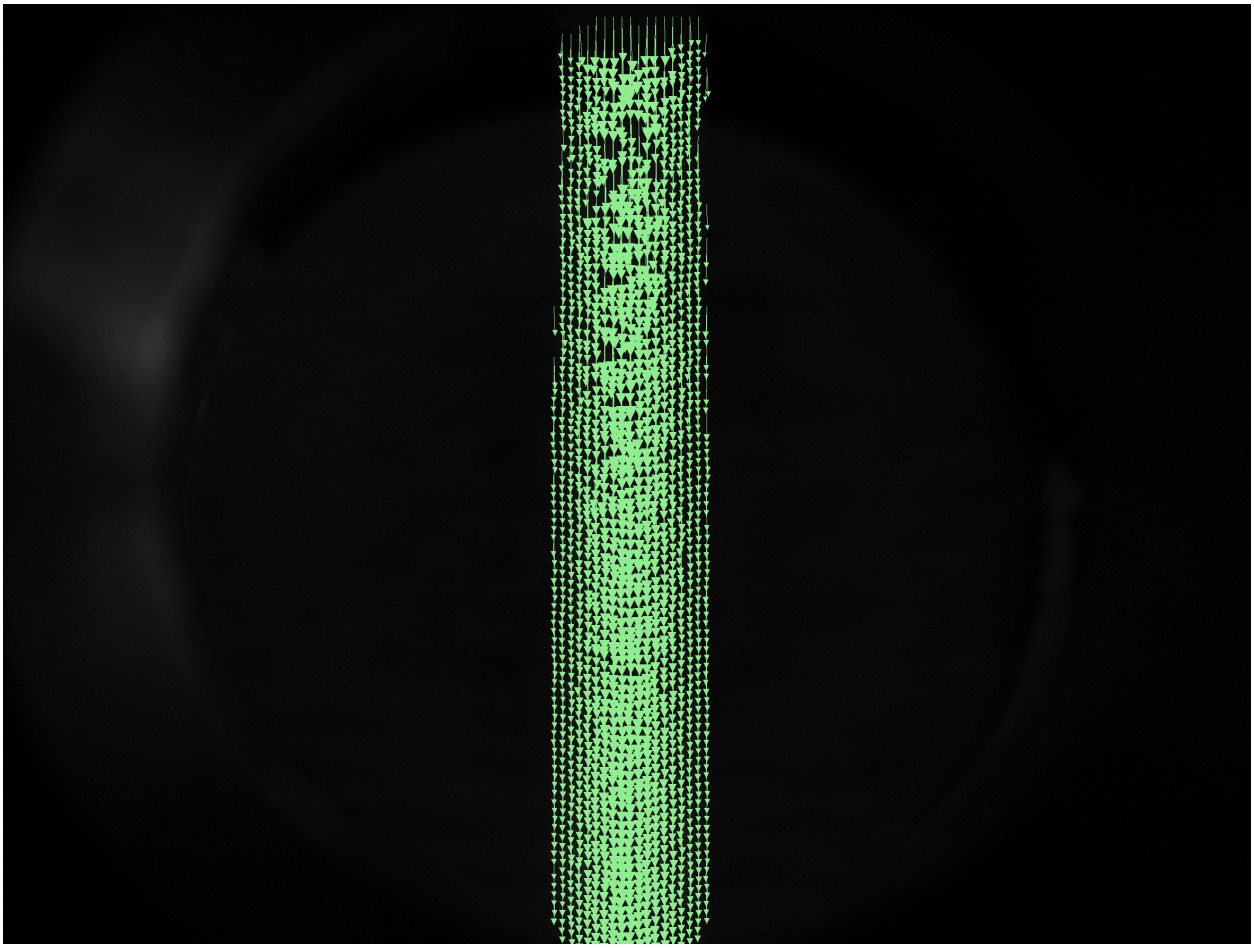

Figure 3.1.2: Initial condition of interface using PIV

the margin to capture an image is very narrow. For a Mach 1.66 shock wave the maximum possible interface velocity is estimated to travel approximately 300 m/s. The critical period of time to capture an interface in any window is about 250 μs of time. Knowing the distance between the location of the preshocked interface and the camera downstream, kinematic equations can be used to determine at what time the interface will enter the field of view. Combining these two times gives the total camera delay time that is entered into Insight. There is however some trial and error involved. This method of anticipating where the interface is at any given time is under ideal conditions, in real world experiments the delay times are slightly off, but they do indicate a good starting point. For a given calculated time, if the interface is not in the frame of the picture, this would indicate that the interface had

not reached the camera's field of view. Therefore, the delay time will be increased by a few hundred microseconds. If however the image showed particles scattered in frame but not a concentrated interface, then the timing was too late and the interface had already passed. So the delay time would be again adjusted to capture an image at a slightly earlier time. The reason for this discrepancy in delay times is a result of the interface nozzles. The inlet is a 0.5 inch diameter nozzle and the exit is a 0.9 inch diameter nozzle. When the shock wave passes over these cavities, mass will escape and weaken the shock wave. While the amount of mass loss is not significant, it is enough to affect the post shock velocity of the interface. It was found for these experiments the interface velocity is around 275 m/s as opposed to 300 m/s, this is only an 8.3 percent error from the theoretical value but it must be compensated for the camera timing.

3.2 Experimental Methods

The experiments run in this study used nitrogen as the driver gas. The driven section is filled with either air or nitrogen gas. The reason these gases were chosen for this study is because of their availability from gas suppliers, in the case of air the supply was free since various parts of the lab have air outlets readily available. Most of these experiments were conducted with a Mach number of 1.66 ± 0.02. Prior to running experiments the laser was turned on and tested using a calibration block to see if the beam is directly aligned to where the camera will view the interface. Next, the cameras are focused to where the image of the interface would appear when shocked. This is done using the same mentioned calibration block. The aperture is then adjusted to assure an adequate amount of light is reaching the sensor to capture images of the interface. Care must be taken when adjusting the aperture, too much exposure will risk damaging the sensor.

Once the camera and laser are set, the shock tube is filled with gas. The interface is injected using the same nitrogen gas bottle that is used to fill the test section. The flow rate is controlled using digital flow meters, the flow rate must be maintained to assure that the

gas cylinder is laminar when injected into the shock tube. The gas flows through the flow meter and then passes into the water particle box where it is seeded with water droplets. The particle-gas is then injected into the test section of the shock tube where it exits a 0.9 inch hole. The gas is left for a minute or two to assure it has reached steady state, and a few pre-shocked images are taken to make sure that the interface is laminar and stable.

The diaphragms used in this study are .030 polycarbonate sheets which produced a Mach number of 1.66. The diaphragms have a dynamic rupture pressure of around 100 psi. For each experiment the driver was pressurized to 76 psi, this is in order to keep the diaphragm just before static failure. The shock wave is fired under a systematic sequence of valve activations using the LabVIEW program. After the "fire shock" command is initiated, the upstream and downstream valves are shut off. At the same time the boost valve is activated and fully opens for 650 ms. The diaphragm bursts at approximately 500 ms however, 650 ms is just a precaution to ensure the diaphragm ruptures under dynamic loading. The shock wave is formed in the driven section and the wave speed is measured using the two DPTs that are spaced 4 inches apart. The post shock data is analyzed to find the two consecutive steep rise in pressure. The first rise in pressure is used to trigger the LabVIEW hardware for the camera and lasers, the delay times that were set previously will capture the images of the interface at the respective windows. Once the experiment is complete the shock tube is vented and depressurized from the driver section using a pressure release valve.

3.3 Qualitative observations of interface evolution

3.3.1 Low Particle Atwood Number

Initial experiments of the flow morphology resulted in unusual evolutions. The experiments conducted in this section used a Mach 1.66 shock wave. The seeded gas used was nitrogen with water particles and the surrounding gas was air. The fact that the densities of air and nitrogen (1.204 kg/m^3 and 1.165 kg/m^3) are not exactly the same are part of the reason for these unique observations. Furthermore, in these experiments the particle delivery

system would lose many particles as they were traveling into the test section, this was due to the solenoid valve that was placed just before entering the test section. This resulted in a low effective Atwood number, of around -0.01. The solenoid valve was later removed and the particle concentration increased considerably, the results from that experimental apparatus are covered in the next section. Originally these results were not intended, however in the interest of studying SDMI these particular experiments reveal some interesting behavior. Due to the configuration of the shock tube at the time, the only images available in this particular experiment are at 0.70 ms and 2.9 ms after shock.

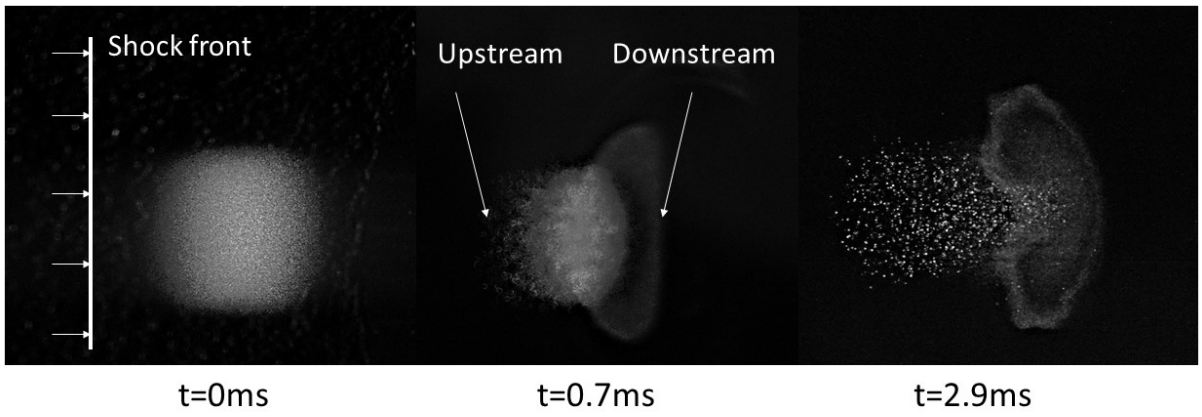

Figure 3.3.1: Mosaic of evolving interface with low atwood number

Looking at figure 3.5.1 for t = 0.7ms the large particles are clearly trailing behind the carrier gas. As specified in section 2.2.2 the particle nebulizers create a mean diameter of 2 microns, they do however also create larger and smaller particles. As a result the observations here are showing how the particles lag with different size; larger particles lag more than smaller particles. There is a faint haze at the downstream location of the interface, this is an instability beginning to develop. The smaller particles are being pulled into this

developing instability. At 2.9 ms, the interface has stretched a considerable amount. The larger particles have almost completely separated from the smaller particles and the vortex pair seen at 0.7ms has become much more pronounced. Smaller particles are being pulled into the vorticies, whereas larger particles are forming a large tail training behind the instability. The majority of the particles have evaporated at this evolution in time, this is supported by the fact that the interface is considerably dimmer and there are fewer particles visible.

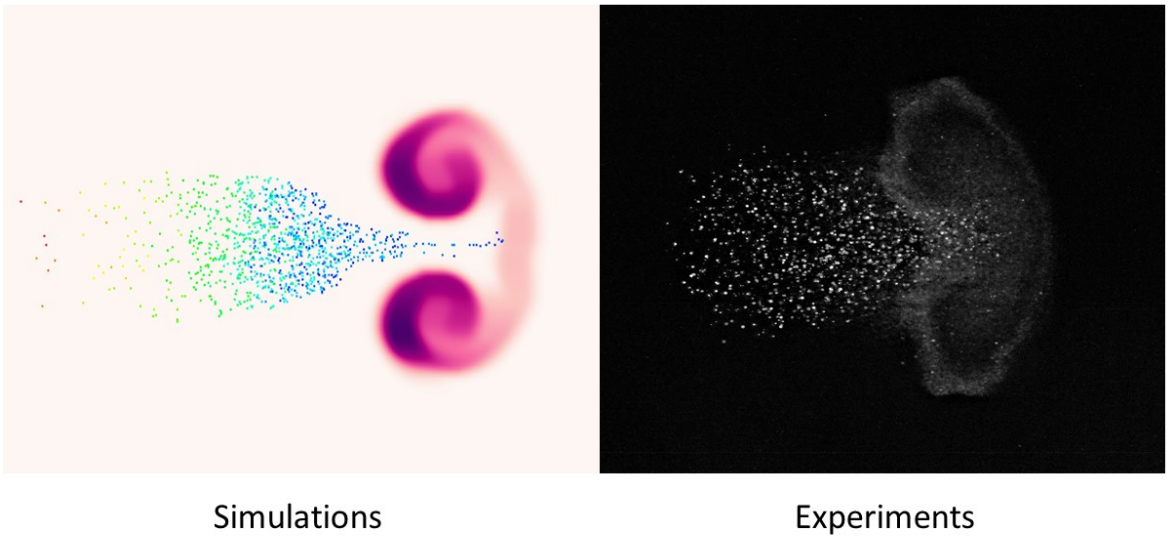

Figure 3.3.2: Comparison of simulation and experimental result for a low Atwood number

Simulations were performed to try and understand the instability that is occurring. Using the same initial conditions as the ones that were done in the shock tube, the simulations were able to reproduce the results that were observed. A comparison of the simulations and experiments can be seen in figure 3.4.2. Much like in the experiments, the larger particles, in red and yellow, are trailing behind the interface. The purple vortex pair is due to the mixing between nitrogen and air. The darker purple represents a higher concentration of nitrogen mixed with the air. The same vorticies seen in the experiments is most likely driven by the mixing of nitrogen with surrounding air. The reason for these effect is due to the gas

Atwood number dominating over the particle Atwood number. This means the instability observed is a traditional RMI rather than a SDMI

3.3.2 High Particle Atwood Number

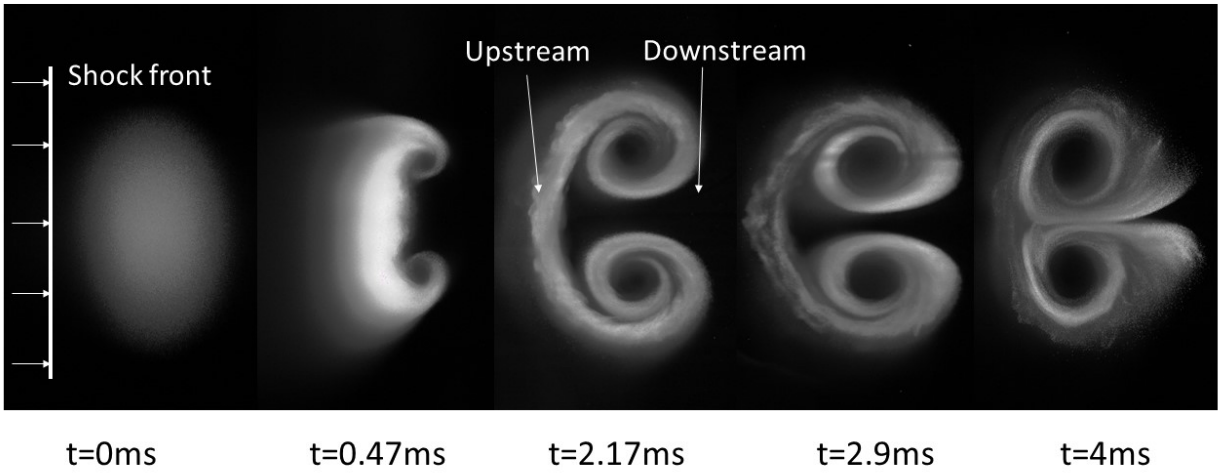

Figure 3.3.3: Mosaic of evolving interface

A higher effective Atwood number was achieved by modifying the PDS with a straight pipe inside the water tank that would extend to just above the water surface, this would insure a maximum particle concentration. The solenoid valve at the test section was also removed to reduce particle losses. The gases used were also the same, giving a gas Atwood number of zero. The times measured in these experiments are taken when the shock wave just reaches the interface to when the evolution of time is 4 ms after shock. The first shocked image of the interface is at 0.47 ms after shock. One feature of this evolution in time is the distinct haze in the upstream location of the interface. As mentioned in the theory, larger particles will lag behind the carrier gas due to momentum. There appears to be a gradient in light intensity as you get further from the interface. The edges of the interface are beginning

to roll up and creating the characteristic vortex pairs seen in a RMI. The slight bump seen between the vortex is the remnants of the initial condition of the interface. The instability forms at the outer edges of the interface and curl inward, this pulls the particles from the center and brings them around the vorticies. Drag causes the piston velocity of the particles to be less than the gas velocity after it is shocked. As indicated by Vorobieff *et al.*[33], The roll-ups seen in this image is a result of the shear acting on the particle interface. The next evolution of time is at 2.1 ms, here the vortex pair is almost perfectly symmetric and well developed. Overall the vortex pairs are smooth at the outer edges of rotation. There seems to be disturbances upstream of the interface. The reasons for this are not known but it could be a secondary instability developing due to either shear effects or 3D effects that cannot be seen in this plane. Traces of lagging particles can still be seen upstream of the interface. At 2.9 ms the vortex pair still has some symmetry. Once again the same disturbances seen in 2.1 ms are seen again. One thing to note is the upstream part of the interface seems to be breaking up. As the interface develops over time, more of the particles in the upstream portion of the interface are being pulled towards the vortex cores. Overall there is a larger concentration of particles in the downstream location of the interface. At 4 ms the entire interface is becoming disordered, while the vortex cores are still distinguishable, the particles around the cores are colliding and bunching up together. Additionally there is an interesting effect occurring, the interface seems to develop certain filament pairs. The particles that make up this shape are considerably further than the interface vortex cores. These filaments are usually observed in a pure RMI, but were previously stated to be non-existant in SDMI [33]. This was originally observed by Vorobieff *et al.*, however, his experiments did not observe later times such as 4 ms, so the filaments observed could be a result of late time developments.

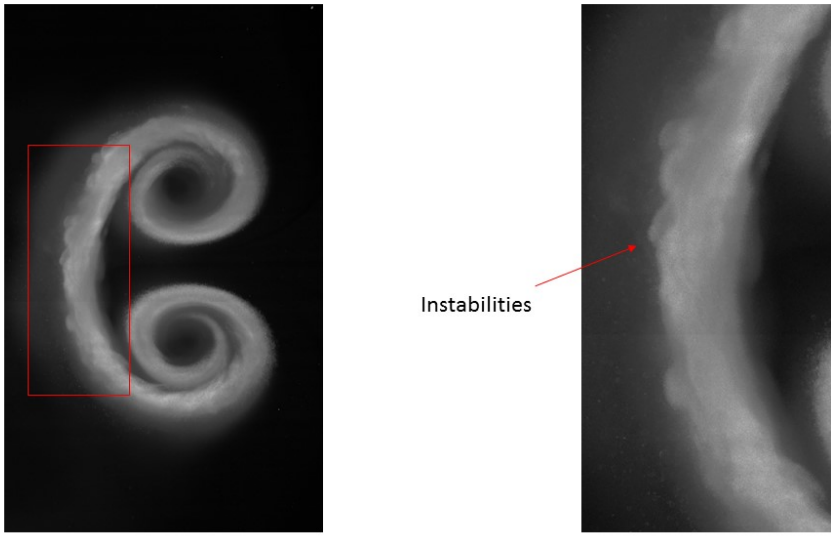

Figure 3.3.4: Detail of interface at 2.1ms

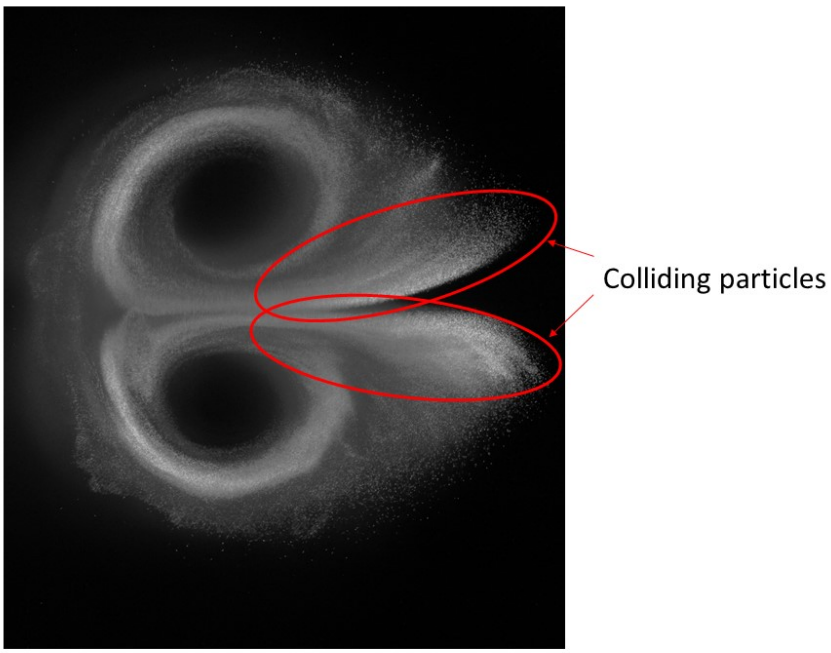

Figure 3.3.5: Detail of colliding particle filaments developing at 4.0ms

3.4 Quantitative observations of interface evolution

Quantitative experimental data was obtained using Insight 4G. While the quality of the images are substantial to gather PIV, many of the post processing settings require knowledge of the program that the author did not have at the time. These PIV images demonstrate the best possible outcome at the time. A PIV image of the interface shown in figure 3.4.1 is at time t = 2.9ms. The green vectors represents "good data"; data points that could easily be calculated from one frame to another. The yellow represents "interpolated data"; this is data that had to be interpolated from one frame to the other. The red vectors represent "bad data" and is typically disregarded in post processing data analysis. A proper data set needs to have approximately 90 percent of all vectors to be in the "good data" category. According to the vector statistics data on Insight for this particular image the percentage of "good vectors", "interpolated vectors", and "bad vectors" is 88, 10, and 2 percent respectively. This indicates that the post processing engine is good enough for getting a good data set. Looking at the image, bad vectors are most prevalent at the inside of the vortex pair. The most likely explanation for this is because there is a low signal to noise ratio in these areas. The cause of this is still yet to be understood but it is most likely due to the processing engine settings. From the PIV vector statistics data, the bulk velocity of the interface is around 277 $\pm$ 2 m/s. This PIV data is valuable because with it the vorticity, circulation, mean velocities, etc. can be calculated and plotted.

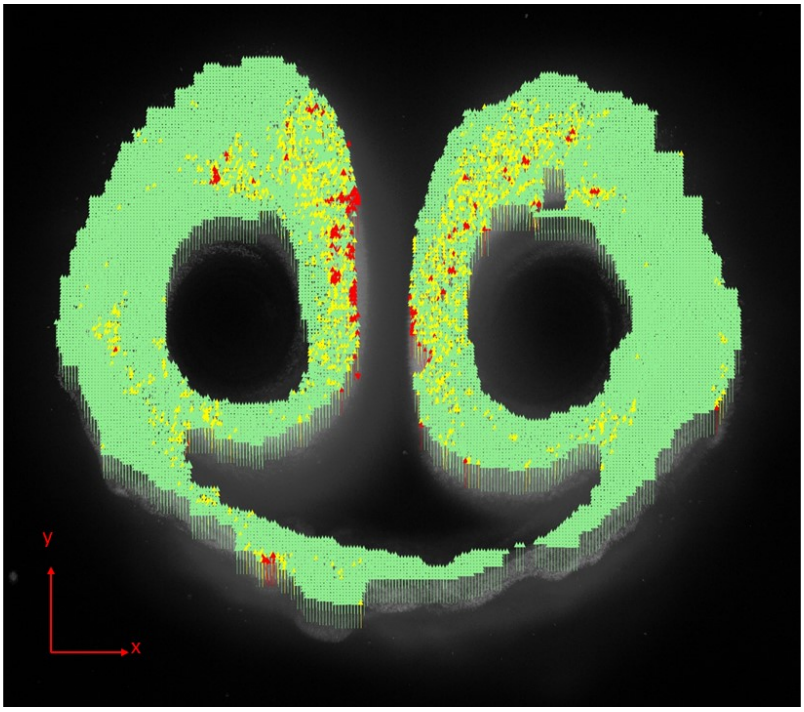

Figure 3.4.1: PIV processed image of shocked interface at 2.9ms

4 Conclusion and Summary

The work presented in this thesis discussed the design, calibration, and experiments of a multiphase shock tube facility. The first chapter went into the theory of multiphase instabilities, 1-D gas dynamics, past literature, and how this work ties into the field of hydrodynamics. The second chapter went into the design of the entire shock tube facility. This included designing the pressure gradient (shock tube), creating the interface, the instrumentation, and laser diagnostics. All parts of the shock tube were analyzed and have a FoS of at least 2. For a maximum Mach number of 2.5, every section of the shock tube is able to withstand pressures felt at this Mach number with the minimum safety factor. The third chapter goes into the methods of calibrating the facility to generating a repeatable shock wave and interface and analyses some of the preliminary data obtained. The test conditions in this study were fo an air-particle gas cylinder shocked with a Mach 1.66 shock wave.

The initial experimental results yielded unusual flow morphology. The PDS used a solenoid valve that restricted flow into the test section, this valve resulted in a considerable amount of particle loss. The gas Atwood number was -0.02, the result of using nitrogen as the test gas and air as the surrounding gas. When experiments were run with this setup the effective Atwood number was about -0.01. The low concentration of particles combined with the dissimilar densities of air and nitrogen resulted in unique instabilities forming, namely the large particles separating from the interface and the small particles being caught into the vortex pairs. Since the gas Atwood number had an overall larger magnitude it dominated the flow morphology, resulting in a RMI instead of a SDMI. The PDS was modified to increase particle concentration and a higher effective Atwood number was achieved, 0.03. Additionally the same gas was used throughout the shock tube eliminating a gas density gradient and only having an effective particle density gradient. The results in this setup agreed with simulations under similar conditions as well as experiments conducted by Vorobieff [33]. Flow morphologies from the shocked interface showed similar vortex pairs forming at corresponding times. Furthermore, there appears to be unique secondary instabilities

forming at later times. The instabilities at 2.1ms are a result of 3D effects of the particles interacting with the surrounding gas. At 4ms colliding particles formed long symmetric filaments. These filaments were once thought to only occur in a pure RMI, however they are appearing at later times in the vortex formation.

For future work the shock tube will continue to be used in investigating SDMI. In particular, the effects of greater particle lag and evaporation are of considerable interest when the flow is reshocked. These conditions closely resemble supernovae explosions in the cosmos and have not been experimentally studied in great detail. Furthermore, preliminary research in plasma generation is being studied by a separate group within the Mizzou FMSTL. This research group will use the shock tube to investigate the effects of accelerating a plasma to understand Magnetohydrodynamcis (MHD).

References

[1] Robert D Richtmyer. Taylor instability in shock acceleration of compressible fluids. *Communications on Pure and Applied Mathematics*, 13(2):297–319, 1960.

[2] EE Meshkov. Instability of the interface of two gases accelerated by a shock wave. *Fluid Dynamics*, 4(5):101–104, 1969.

[3] David Arnett. The role of mixing in astrophysics. *The Astrophysical Journal Supplement Series*, 127(2):213, 2000.

[4] Jochen Krebs and Wolfgang Hillebrandt. The interaction of supernova shockfronts and nearby interstellar clouds. *Astronomy and Astrophysics*, 128:411–419, 1983.

[5] Joseph Yang, Toshi Kubota, and Edward E Zukoski. Applications of shock-induced mixing to supersonic combustion. *AIAA journal*, 31(5):854–862, 1993.

[6] K Kailasanath. Liquid-fueled detonations in tubes. *Journal of Propulsion and Power*, 22(6):1261–1268, 2006.

[7] Kishore Nekkanti. Analysis of thrust development in a pulse detonaton engine. 2010.

[8] Arun K Sehra and Woodrow Whitlow. Propulsion and power for 21st century aviation. *Progress in Aerospace Sciences*, 40(4):199–235, 2004.

[9] Andrzej Gardzilewicz, Michal Kolovratnik, et al. Numerical and experimental investigations of steam condensation in lp part of a large power turbine. *Journal of Fluids Engineering*, 131(4):041301, 2009.

[10] Kenneth H Wohletz. Mechanisms of hydrovolcanic pyroclast formation: grain-size, scanning electron microscopy, and experimental studies. *Journal of Volcanology and Geothermal Research*, 17(1):31–63, 1983.

[11] RC Ripley and F Zhang. Jetting instability mechanisms of particles from explosive dispersal. In *Journal of Physics: Conference Series*, volume 500, page 152012. IOP Publishing, 2014.

[12] Jacob A McFarland, Wolfgang J Black, Jeevan Dahal, and Brandon E Morgan. Computational study of the shock driven instability of a multiphase particle-gas system. *Physics of Fluids*, 28(2):024105, 2016.

[13] John D. Anderson. *Modern Compressible Flow with Historical Perspective*. McGraw Hill, third edition, 2003. pg. 274–298.

[14] A Benuzzi-Mounaix, M Koenig, A Ravasio, T Vinci, N Ozaki, M Rabec le Gloahec, B Loupias, G Huser, E Henry, S Bouquet, et al. Laser-driven shock waves for the study of extreme matter states. *Plasma physics and controlled fusion*, 48(12B):B347, 2006.

[15] Harry F Robey, JO Kane, BA Remington, RP Drake, OA Hurricane, H Louis, RJ Wallace, J Knauer, P Keiter, D Arnett, et al. An experimental testbed for the study of hydrodynamic issues in supernovae. *Physics of Plasmas*, 8(5):2446–2453, 2001.

[16] Elijah Courtney, Amy Courtney, and Michael Courtney. Shock tube design for high intensity blast waves for laboratory testing of armor and combat materiel. *Defence Technology*, 10(2):245–250, 2014.

[17] P Wayne, D Olmstead, P Vorobieff, CR Truman, and S Kumar. Oblique shock interaction with a cylindrical density interface. *Computational Methods in Multiphase Flow VIII, editors: CA Brebbia, P. Vorobieff. JL Muñoz-Cobo, WIT Press, Southampton, UK*, pages 161–170, 2015.

[18] Martin Brouillette and B Sturtevant. Experiments on the richtmyer–meshkov instability: Small-scale perturbations on a plane interface. *Physics of Fluids A: Fluid Dynamics*, 5(4):916–930, 1993.

[19] JW Jacobs. The dynamics of shock accelerated light and heavy gas cylinders. *Physics of Fluids A: Fluid Dynamics*, 5(9):2239–2247, 1993.

[20] PM Rightley, P Vorobieff, R Martin, and RF Benjamin. Experimental observations of the mixing transition in a shock-accelerated gas curtain. *Physics of Fluids*, 11(1):186–200, 1999.

[21] GC Orlicz, BJ Balakumar, CD Tomkins, and KP Prestridge. A mach number study of the richtmyer–meshkov instability in a varicose, heavy-gas curtain. *Physics of Fluids*, 21(6):064102, 2009.

[22] Jacob Andrew Mcfarland. *Experimental and Computational Study of the Inclined Interface Richtmyer-Meshkov Instability*. PhD thesis, Texas A&M University, 2013.

[23] Jacob McFarland, David Reilly, Skylar Creel, Christopher McDonald, Thomas Finn, and Devesh Ranjan. Experimental investigation of the inclined interface richtmyer–meshkov instability before and after reshock. *Experiments in fluids*, 55(1):1640, 2014.

[24] Bradley Motl, Jason Oakley, Devesh Ranjan, Chris Weber, Mark Anderson, and Riccardo Bonazza. Experimental validation of a richtmyer–meshkov scaling law over large density ratio and shock strength ranges. *Physics of Fluids*, 21(12):126–102, 2009.

[25] BD Collins and JW Jacobs. Plif flow visualization and measurements of the richtmyer–meshkov instability of an air/sf 6 interface. *Journal of Fluid Mechanics*, 464:113–136, 2002.

[26] Jeffrey W Jacobs. Shock-induced mixing of a light-gas cylinder. *Journal of Fluid Mechanics*, 234:629–649, 1992.

[27] JW Jacobs. Shock accelerated cylindrical gas inhomogeneities. part 2-a heavy gas cylinder. 1993.

[28] S Kumar, G Orlicz, C Tomkins, C Goodenough, K Prestridge, P Vorobieff, and R Benjamin. Stretching of material lines in shock-accelerated gaseous flows. *Physics of Fluids*, 17(8):082107, 2005.

[29] Joseph Conroy. *Planar shock wave interaction with a multiphase cylinder*. PhD thesis, 2012.

[30] S Kumar, P Vorobieff, G Orlicz, A Palekar, C Tomkins, C Goodenough, M Marr-Lyon, KP Prestridge, and RF Benjamin. Complex flow morphologies in shock-accelerated gaseous flows. *Physica D: Nonlinear Phenomena*, 235(1):21–28, 2007.

[31] C Tomkins, K Prestridge, P Rightley, M Marr-Lyon, P Vorobieff, and R Benjamin. A quantitative study of the interaction of two richtmyer–meshkov-unstable gas cylinders. *Physics of Fluids*, 15(4):986–1004, 2003.

[32] M Anderson, Peter Vorobieff, CR Truman, C Corbin, G Kuehner, P Wayne, J Conroy, R White, and S Kumar. An experimental and numerical study of shock interaction with a gas column seeded with droplets. *Shock Waves*, 25(2):107–125, 2015.

[33] Peter Vorobieff, Michael Anderson, Joseph Conroy, Ross White, C Randall Truman, and Sanjay Kumar. Vortex formation in a shock-accelerated gas induced by particle seeding. *Physical Review Letters*, 106(18):184503, 2011.

[34] Richard G. Budynas and J. Keith Nisbett. *Mechanical Engineering Design*. McGraw Hill, ninth edition, 2008.

[35] Chen S Tsai, Rong W Mao, Shirley C Tsai, Kaveh Shahverdi, Yun Zhu, Shih K Lin, Yu-Hsiang Hsu, Gerry Boss, Matt Brenner, Sari Mahon, et al. Faraday waves-based integrated ultrasonic micro-droplet generator and applications. *Micromachines*, 8(2):56, 2017.

[36] Walker Bleakney, DK Weimer, and CH Fletcher. The shock tube: a facility for investigations in fluid dynamics. *Review of Scientific Instruments*, 20(11):807–815, 1949.

[37] William Adolph Crede. The design and construction of a shock tube facility. 1965.

[38] Jeevan Dahal. *Numerical method for shock driven multiphase flow with evaporating particles*. PhD thesis, University of Missouri–Columbia, 2016.